ORIGINAL PAPER



Phenotypic trait of particle geometries

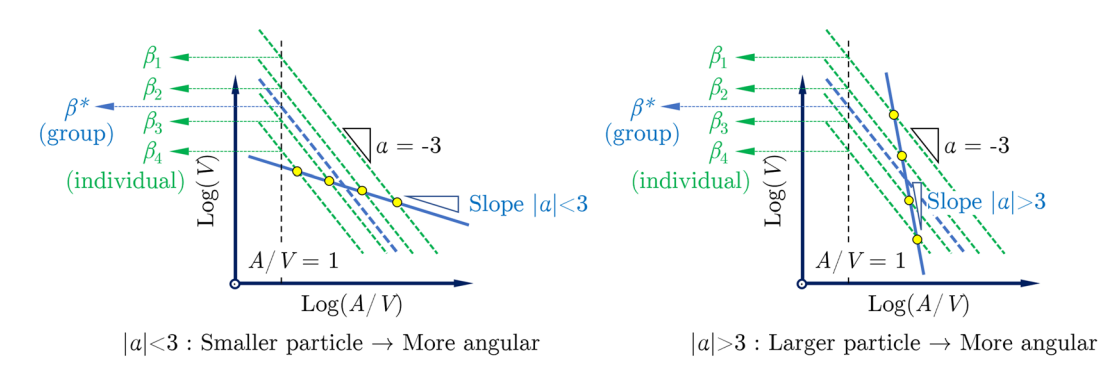
Seung Jae Lee¹ · Moochul Shin² · Chang Hoon Lee² · Priya Tripathi¹

Received: 13 October 2021 / Accepted: 28 April 2022 © The Author(s), under exclusive licence to Springer-Verlag GmbH Germany, part of Springer Nature 2022

Abstract

People of a race appear different but share a 'phenotypic trait' due to a common genetic origin. Mineral particles are like humans: they appear different despite having a same geological origin. Then, do the particles have some sort of 'phenotypic trait' in the geometries as we do? How can we characterize the phenotypic trait of particle geometries? This paper discusses a new perspective on how the phenotypic trait can be discovered in the particle geometries by quantifying the 'variation' and 'average' of the geometry. The key idea is using the power-law relation between particle surface-area-to-volume ratio (A/V) and the particle volume (V) that uncovers the phenotypic trait in terms of α and β *: From the power regression between A/V and V in a log-log space, the power value (slope) α represents the relation between shape and size, while β * (intercept of the power regression evaluated by fixing α = -3) informs the angularity of the average shape in the granular material. In other words, α represents the 'variation' of the geometry, while β * is concerned with an 'average' geometry of a granular material. Furthermore, this study finds that A/V and V can also be used to characterize 'individual' particle shape in terms of Wadell's true Sphericity (S). This paper also revisits the $M = A/V \times L/6$ concept originally introduced by Su et al. [Transp. Geotech. 23: 100328, 2020] and finds the shape index M is an extended form of S providing additional information about the particle elongation. Therefore, the proposed method using A/V and V provides a unified approach that can characterize the particle geometry at multiple scales from a granular material to single particle.

Graphical abstract



• : Data points

 $\beta_{i=1,2,...}$: Angularity of individual particle (= A^3/V^2 ; the higher β value, the more angular the shape)

 β^* : Average shape angularity of the particles in the group $(\beta^*=10^{\overline{\text{Log}(\beta_i)}})$ where $\overline{\cdots}$ is the mean of \cdots)

 S^{I} : Wadell's true Sphericity (= $A/V \times D/6$; shape as a function of surface area A, volume V, and size D)

M: Shape index $(= A/V \times L/6)$, thus M/S^{-1} presents the particle elongation.

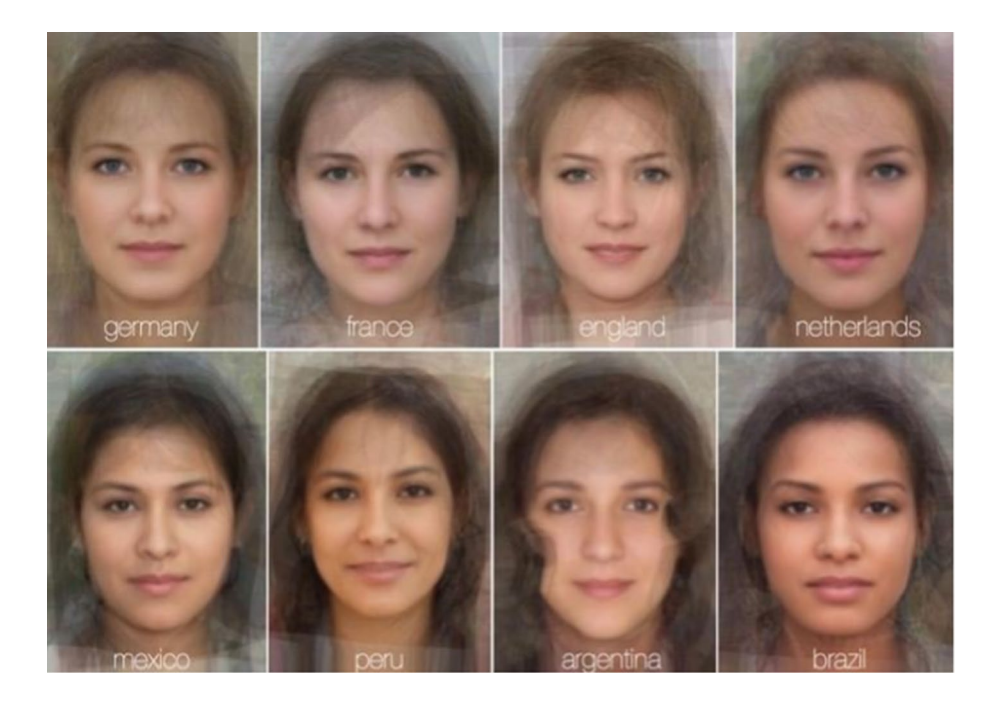
Keywords Particle geometry · Power law · Wadell's true Sphericity · M-A-V-L

Extended author information available on the last page of the article

Published online: 10 June 2022



Fig.1 Average face of women in some countries (Image used under CC-BY-4.0 license [8])



List of symbols

- α Slope of a power regression of A/V and V data points in a log-log space; α indicates the particle shapesize relation of a granular material
- β Geometry constant that indicates the 'individual particle' angularity
- β_n Normalized β indicating individual particle's relative angularity compared to sphere; See Eq. (6)
- β^* Intercept of a power regression at A/V = 1 evaluated with α fixed at -3; This β^* indicates the angularity of the average particle shape in a 'granular material'
- β^*_n Normalized β^* indicating the relative angularity of particles in a granular material compared to sphere; See Eq. (10)
- $\overline{\beta}$ Arithmetic mean of β (which is different from β^*)
- β^a 'Actual' intercept of a power regression at A/V=1
- ψ Friction angle per notation in [45]
- A Particle surface area
- A_s Surface area of a reference sphere having the same volume as the particle
- D Diameter of a reference sphere having the same volume as the particle
- L Diameter of particle's circumsphere (circumdiameter)
- M Morphology index obtained by $M = A/V \times L/6$
- S Wadell's true Sphericity; An inverse of S (i.e., S^{-1}) is obtained by $S^{-1} = A/V \times D/6$
- V Particle volume

1 Introduction

The 3D particle geometry (i.e., shape, volume, surface area, and size) is fundamental information to understand the physical properties and behavior of granular materials [2–6]. Typically, mineral particles usually come in a variety of shapes and sizes. In a sense, mineral particles are like humans: people of a race may not look alike and typically have some variations in their appearances despite a common genetic origin. Likewise, mineral particles look different even if they have a same geological origin. However, people share a 'phenotypic trait' and the 'average face' may be found from each race [7, 8] as shown in the examples of Fig. 1. Then, we can ask some questions: Is there a phenotypic trait in the particles we can find in terms of the 'average' geometry? Also, how can we systematically quantify the geometric 'variation' in the particles? Researchers attempted to answer these questions. For example, Alderliesten [9–18] performed extensive statistical studies of the different types of size measurements and combinations of those, suggesting a set of 'mean particle diameters'. However, these studies did not take the particle shape into account, which is a major limitation.

It is important to address the 'variation' and 'average' of particle geometries including the shape, e.g., to effectively model the particles and simulate the granular material behavior using the discrete element method (DEM). Although the simulation fidelity of granular material behavior could have been greatly enhanced with the recent advances in computing resources and modeling techniques, there are still large gaps in accurately modeling the mineral



particles for DEM analysis [19–22]. For example, every mineral particle in the field looks different in terms of shape and size, then how can we model all different particles for the DEM simulation? If it is impractical to model all of those, then how many shapes do we need to model to make DEM simulation as accurate as possible? Is there a systematic way we can use to identify some representative shapes for the modeling? In general, the particle shape changes with size, then how can we effectively model this?

To address these questions, this paper proposes a new approach using a power-law between particle surface-areato-volume ratio (A/V) and the particle volume (V) which is the key information to uncover the phenotypic trait (i.e., average and variation) of particle geometries of a granular material. In addition, this paper demonstrates Wadell's true Sphericity (S) – that characterizes the 'individual' particle shape – can be also quantified in terms of A/V and V. Therefore, A/V and V can be consistently used to describe the particle geometry at multiple scales from a granular material to single particle. Furthermore, this paper discusses that $M = A/V \times L/6$ concept introduced by Su et al. [1] is an extended form of S that provides the additional information about the particle elongation. There are indeed many 2D and 3D shape indices that have been developed in the research community nearly for a century to quantify the shape properties such as sphericity, roundness, aspect ratio, convexity, etc. [23–31]. Various versions of the shape index have been developed to measure each shape property, e.g., five different sphericities are broadly used in the engineering practice [32–34]. The literature on this subject is vast. A comprehensive review of the conventional shape indices is provided in [35–37]. Compared to the conventional shape indices, the advantage of the $M = A/V \times L/6$ concept is that the particle shape is quantified as a function of the other geometry parameters (i.e., surface area A, volume V, and size *L*) which therefore enables to interpret the interrelation of those fundamental properties. These four parameters are inherently coupled, e.g., if mineral particles are weathered, the particles change to a more rounded shape as well as the volume, surface area, and size. Likewise, if a particle is crushed, all these four parameters change together. While the particle shape effect on the granular material behavior has been extensively studied in the research community, we need to look at the 'shape effect' a little more carefully because the shape effect cannot be isolated and is triggered by any of the geometry parameters. This $M = A/V \times L/6$ approach explains how volume relates to surface area and size for irregularly shaped particles in general, allowing for a better understanding of the overall particle geometry effect on the complex macroscopic behavior of granular materials.

Section 2 discusses the use of the power law between A/V and V to identify the phenotypic trait of granular material (i.e., a group of particles). Section 3 shows examples of the

proposed approach applied to a larger number of artificially generated and mineral particles. Section 4 discusses the use of individual A/V and V data to identify the shape of single particle.

2 Phenotypic trait of granular material

The particle surface-area-to-volume ratio (A/V) is the key information to characterize the particle shape [1]. The A/V ratio is also called the 'specific surface area per unit volume' which is considered an important particle-scale property that governs the physical phenomena of solids and granular materials such as modulus, strength, permeability, and transport processes [38, 39]. The relation between A/V and particle volume (V) of a granular material (i.e., a group of particles) can be approximated by a 'power-law' [40]. We find this relation between A/V and V space can be used to uncover the 'phenotypic trait' of the particle geometries in a granular material.

As a starter, the relation of particle A/V and V can be formulated as below. Particle volume (V) is a 3-dimensional measure and particle surface area (A) is a 2-dimensional measure. Therefore, the relation between A and V can be shown as in Eq. (1), where λ is a constant that depends on the particle geometry. Equation (1) can be reformulated to Eq. (2) in terms of A/V and V, and $1/\lambda^2$ is replaced with β in Eq. (3). Therefore, β is equal to A^3/V^2 as in Eq. (4). This β increases with the particle angularity, e.g., β is 36π for sphere, 216 for cube and 374.12 for tetrahedron. Therefore, the individual particle's angularity may be expressed by β . This power-law relation between A/V and V can be log-transformed as in Eq. (5). The β may be normalized to β_n as in Eq. (6) to indicate the relative angularity to sphere. Therefore, β_n is 1.00 for sphere, 1.91 for cube and 3.31 for tetrahedron.

$$V = A^{3/2} \times \lambda \tag{1}$$

$$V = (A/V)^{-3} \times 1/\lambda^2 \tag{2}$$

$$V = (A/V)^{-3} \times \beta \tag{3}$$

$$\beta = A^3/V^2 \tag{4}$$

$$\log(V) = -3 \times \log(A/V) + \log(\beta) \tag{5}$$

$$\beta_n = \beta / (36\pi) = (A^3/V^2) / (36\pi)$$
 (6)

¹ Throughout this paper, the common logarithm (base 10) is considered, and we omit writing of the base 10 in the logarithm notation.



79 Page 4 of 25 S. J. Lee et al.

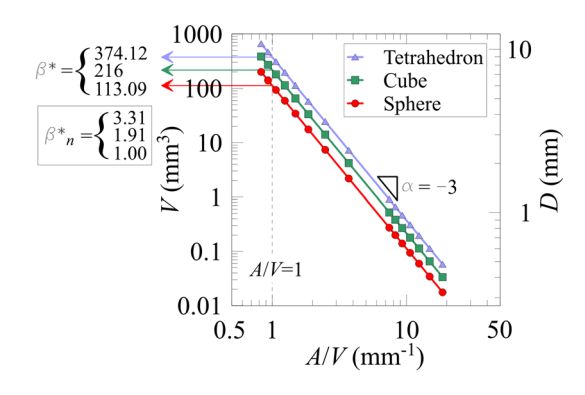


Fig. 2 Power regression for the three groups of particles with an identical shape

2.1 Case 1: Particles of an identical shape

The log-transformed relation of A/V and V is linear as in Eq. (5), implying that the slope of the power regression of the data points is -3 in a log-log space if all particles in a granular material have a same shape. Figure 2 shows an example in which the A/V and V values of three particle groups are plotted in a log-log space. Each group has an identical shape: Group 1 is composed of 15 spheres, Group 2 has 15 cubes, and Group 3 has 15 regular tetrahedrons. The particles in each group have various sizes of about $0.3 \sim 10$ mm measured in terms of the size D. The size D is the diameter of a reference sphere having the same volume as the particle, which can be analytically obtained as in Eq. (7). The geometric properties of all particles are presented in Table 1, 2 and 3 in Appendix.

$$D = 2 \times (3V/(4\pi))^{1/3} \tag{7}$$

As shown in Fig. 2, the A/V and V relation is linear in a log-log space, which can be approximated with a power function. The slope of the power regression is invariably -3 for every group with no variance. Hereafter, α denotes the slope of the power regression. Thus, $\alpha = -3$ if the shape of particles in a granular material is identical. To put it another way, the resulting value of $\alpha = -3$ from the regression can be generalized to 'no specific relation between shape and size' since there is only one shape in the particle group. In Sect. 2.2, we will further generalize the idea of how α varies as the shape changes with size.

The β is defined for a 'single particle' as in Eq. (4). Similarly, β^* is defined for a 'group of particles' which can be obtained from the power regression with the plot's *intercept* at A/V=1. If all particles have a same shape, β of all particles are same, thus naturally $\beta^*=\beta$. For multiple particles, β^* can be analytically obtained as in Eq. (8), translating to that β^* is the intercept of power regression evaluated with

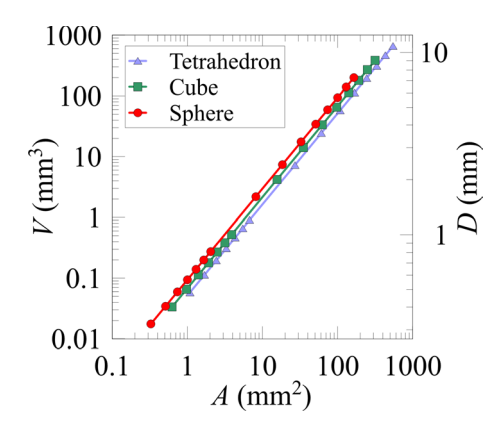


Fig. 3 Power regression in an A and V space

a fixed value of $\alpha = -3$. The intercept β^* also increases with the overall angularity of particle geometries like β . The β^* is 113.09 (=36 π) for spherical particles (Group 1), 216 for cubes (Group 2) and 374.12 for regular tetrahedra (Group 3) as shown in Fig. 2. Considering the β^* is defined for a group of particles, the β^* informs the average shape angularity of the particles. This will be further discussed in Sect. 2.2.

$$\beta^* = 10^{\overline{\log(\beta)}} = 10^{\overline{\log(V) + 3 \times \log(A/V)}}$$
(8)

where $\overline{\cdots}$ indicates the arithmetic mean of \cdots .

It is worth noting that β^* is not the arithmetic mean of β . Equation (9) shows the definition of $\overline{\beta}$ (the arithmetic mean of β) which is different from β^* in Eq. (8). Therefore, $\overline{\beta}$ does not represent the intercept of the power regression.

$$\overline{\beta} = \overline{10^{\log(\beta)}} = \overline{10^{\log(V) + 3 \times \log(A/V)}} \tag{9}$$

where $\overline{\cdots}$ indicates the arithmetic mean of \cdots .

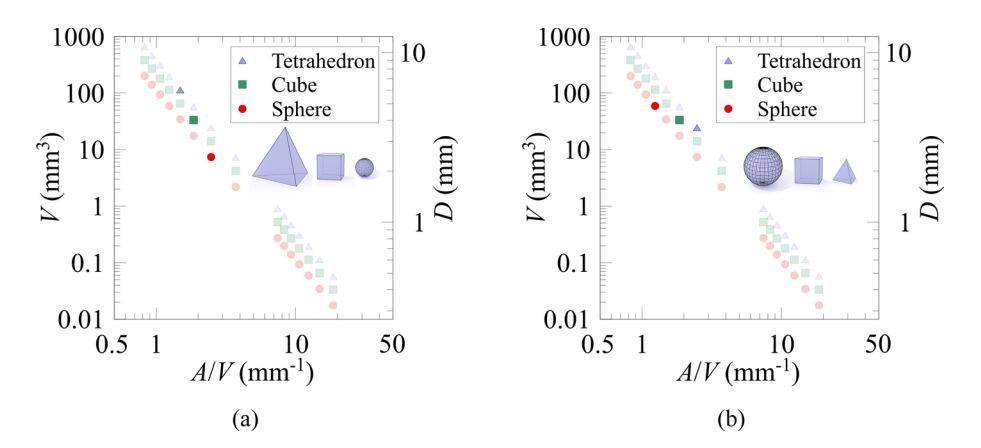
As β_n indicates the individual particle's relative angularity to sphere as in Eq. (6), β^*_n can be similarly defined for a group of particles as in Eq. (10). Note that if the shape of particles is the same in a group, $\beta^*=\beta$, thus $\beta^*_n=\beta_n$.

$$\beta_n^* = \beta^* / (36\pi) \tag{10}$$

As a side note, readers may wonder why Eq. (2) is log-transformed (i.e., in terms of A/V and V) instead of Eq. (1). A main reason is that the A/V ratio is an important particle-scale property often called the 'specific surface area per unit volume' as discussed at the beginning of Sect. 2. Therefore, formulation using the A/V ratio will enable to facilitate the interpretation of the associated physical phenomena. Another reason is that the data points tend to be less discriminated when using Eq. (1). For example, Fig. 3 shows the power regression in an A and V space where the data points are less distinct compared to Fig. 2. The intercept



Fig. 4 Two groups of particles with three different shapes: **a** Group A – the more angular shape is larger; **b** Group B – the shape-size relation is the opposite to Group A



values (that correspond to β^*) also tend to be too small which are 0.094, 0.068, 0.052 for sphere, cube, and tetrahedron, respectively. Use of either Eq. (1) or (2) may be a matter of preference. Nevertheless, it is noted that a different interpretation is certainly required when using Eq. (1), e.g., the slope of the log-transformed equation changes to 3/2.

2.2 Case 2: Particles with different shapes

The next question is how α and β^* would change when particles have different shapes. Group A and B are created as example particle groups having different shapes. Each group consists of three particles (a regular tetrahedron, a cube, and a sphere) selected from the three-shape groups presented in Sect. 2.1. The difference between Group A and B is the relation of shape and size: in Group A, the more angular the shape is, the larger the size is (i.e., tetrahedron is the largest, cube is the next, and sphere is the smallest). On the other hand, Group B is the opposite (i.e., sphere is the largest, cube is the next, and tetrahedron is the smallest). In the context, it is noted that "large/small" is defined by the volume of each particle. In Fig. 4a and b, the size of three particles is schematically shown and the corresponding data points are highlighted with darker colors. The geometric properties of particles in Group A and B are presented in Table 4.

2.2.1 α : Indication of shape-size relation

Figure 5 shows the power regressions for both groups. Here we can see that the power value α (slope) is not -3 for both groups. As shown for Group A (α = -5.34), when α is less than -3 ($|\alpha|$ > 3), the slope is steeper, implying that the larger particles are more angular than smaller ones. In Group B (α = -1.28), when α is greater than -3 ($|\alpha|$ <3), the slope is gentle, indicating that the smaller particles are more angular. On the other hand, α = -3 indicates there is no particular relation between the shape and size. For example, the resulting slope α is equal to -3 from the regression if all 45 particles are considered (the dashed line in Fig. 5) because the

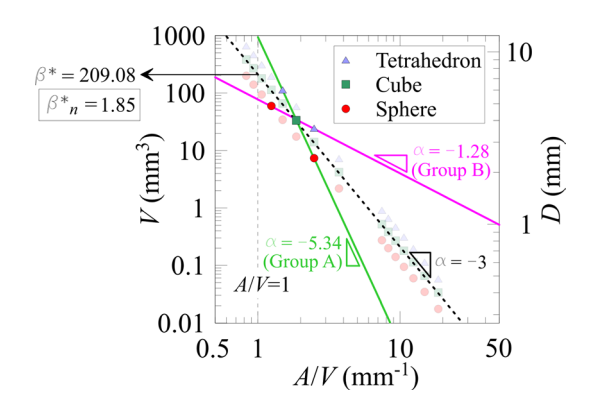


Fig. 5 Power regression for the two groups of particles with different shapes

composition of the particle shapes (i.e., tetrahedron, cube, and sphere) do not change with size. This can be considered as a generalization of the case in Sect. 2.1.

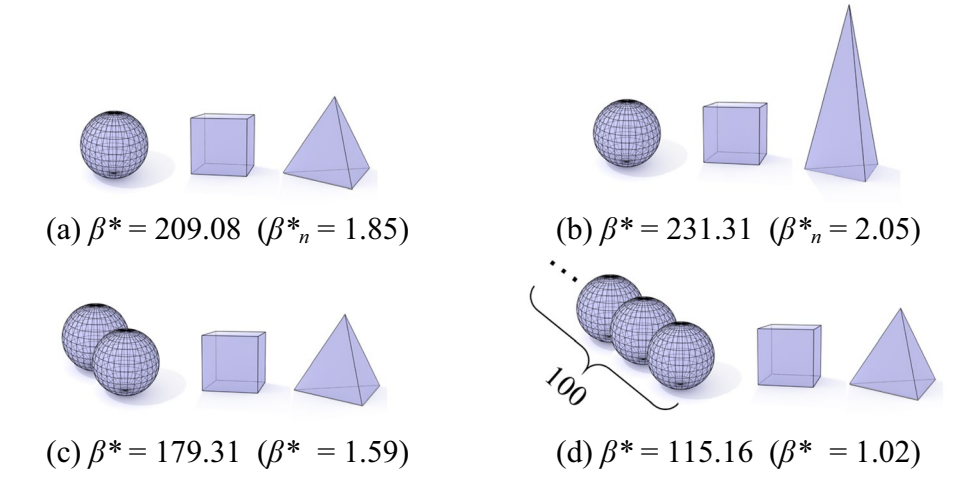
2.2.2 β *: Indication of average shape angularity

The β^* is evaluated with a fixed value of $\alpha = -3$ as in Eq. (8) and concerned with the average of particle geometries. The β^* has three properties as below.

First, β^* represents the average shape angularity. The β^* obtained for all 45 particles is 209.08 as shown in Fig. 5. This β^* informs the angularity of the average particle shape is close to that of the cube, which is 216 (see Fig. 2). This makes sense because (i) the average shape is somewhere halfway between the (least angular) sphere and the (most angular) tetrahedron and (ii) there are equal amounts of sphere, cube and tetrahedron within each group (i.e., 15 particles each). For the same reason, the β^* evaluated for each Group A and B is also equal to 209.08 because there are equal amounts of sphere, cube and tetrahedron within each group (i.e., one particle each). Figure 6 shows other examples of how β^* changes depending on the shapes of the constituent particles. The details of the geometric properties



Fig. 6 Change of β^* with different constituent shapes; In **b**, the length of long edges of the elongated tetrahedron is 3.2 each, and the length of the base edges is 1.5 each



are presented in Table 5. Figure 6a shows $\beta^*=209.08$ as in Group A and B. With an elongated tetrahedron as in Fig. 6b, β^* increases to 231.31. As the elongated tetrahedron has the higher angularity than the regular tetrahedron in Fig. 6a, the average angularity gets higher which is reflected in the higher β^* . To the contrary, if there are two spheres in the group (Fig. 6c), the β^* drops to 179.31, because the additional sphere reduces the angularity of the group on average. The β^* decreases even further with more spheres: With 100 spheres as in Fig. 6d, β^* gets to 115.16. As the spheres are dominant, β^* is now close to 113.09 (= 36 π) of the spheres-only group. As the number of spheres increases, β^* approaches 113.09 (and β^*_n approaches 1) asymptotically.

Second, β^* is scale-free in the sense that β^* is not influenced by the particle size. Graphically, β^* is the intercept at A/V = 1 of the power regression evaluated with a fixed value of $\alpha = -3$. Therefore, if the data points move along the slope α = -3, the regression line does not change, so β * (intercept) does not change either. For example, α is -3 if particles of different sizes have the same shape (Fig. 2). This implies a change in particle size simply makes the data point move along a line with the slope of $\alpha = -3$, which does not change the β^* . Since β^* is evaluated with a fixed value of $\alpha = -3$, the evaluation of β^* is not influenced by particle sizes. Therefore, Group A and B having the same set of particle shapes show the same $\beta^* = 209.08$ despite the different shape-size relations. Figure 6a is a variation of Group A and B with the same set of particle shapes. The only difference is that particles in Fig. 6a have a unit volume (see Table 5). The same β^* is obtained, because the different size has no effect on β^* . For another example, a variation of Fig. 6b is created with arbitrary sizes as in Table 6. The same β *=231.31 is obtained as in Fig. 6b.

Third, β^* is independent of unit. For the same reason that β^* is scale-free as described above, a change of unit simply moves the data point along the slope $\alpha = -3$. Therefore, β^* is not affected by the unit. For example, Fig. 7 shows the

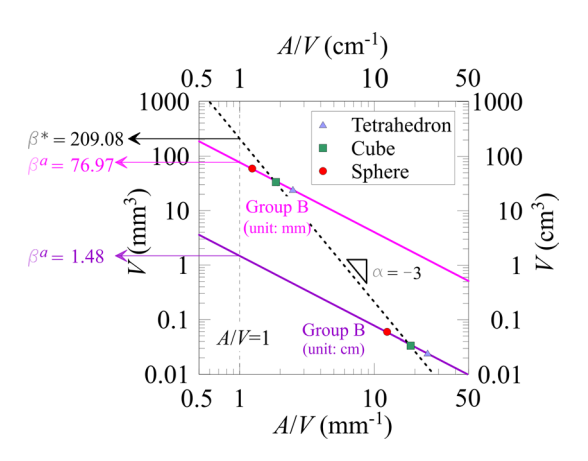


Fig. 7 Group B data in millimeter (mm) and centimeter (cm); β^* is not influenced by the unit

Group B data in both mm and cm, which results in the same $\beta^* = 209.08$ ($\beta^*_n = 1.85$). The data are provided in Table 4.

It is worth noting that the 'actual' intercept of the power regression at A/V = 1 (let us call this β^a) changes with the unit unlike β^* . For example, if 'mm' is used, the power regression of Group B is $V = (A/V)^{-1.28} \times 76.97$, thus the β^a of Group B is 76.97 as shown in Fig. 7. However, if 'cm' is used, the power regression of Group B is expressed as $V = (A/V)^{-1.28} \times 1.48$, thus β^a is now 1.48. This unit dependency makes β^a less universal index. More importantly, β^a also changes with the slope α . Therefore, the β^a does not provide meaningful information related to the angularity of average shape unlike β^* . For example, although the constituent shapes in Group A and B are identical, the different shape-size relations (thus different slope α) change the actual intercept β^a (Fig. 5). Despite Group B has angular shapes in addition to the sphere, β^a of Group B (=76.97) is even lower than that of the spheres-only group (i.e., 113.09).



3 Applications to artificially generated and 3D scanned mineral particles

We demonstrate the evaluation of α and β^* for larger datasets. Section 3.1 analyzes a set of 200 polyhedral particles artificially developed in various shapes and sizes. This set includes near-spherical and angular particles. Section 3.2 analyzes a set of mineral particles after 3D scanning to observe how α and β^* are realized for the real particles. Section 3.3 analyzes fragmented particles which are expected to exhibit the highest β^* value among all three examples due to the presence of angular shapes generated by the breakage.

3.1 Polyhedral particles

A large dataset of 200 polyhedral particles having various shapes and sizes was artificially generated by Su et al. [1]. The particle images are shown in Fig. 8 and the geometry information are summarized in Table 7. This set of particles is composed of two groups: (i) near-spherical (particle ID: 1–100) and (ii) mixed shapes (particle ID: 101–200). When creating the group of mixed shapes, a specific shape-size relation was considered such that the smaller particles tend to have more non-spherical (i.e., angular and/or elongated) shapes.

Figure 9 shows the phenotypic traits of particle geometries from the A/V and V power regression. As shown in the figure, two different traits are clearly seen, indicating two different sets are mixed in the 200 particles. For one group of the data, the evaluated α is -2.99 and β * is 116.29 $(\beta^*_n = 1.03)$, and for the other group, α is -2.64 and β^* is 155.69 ($\beta^*_n = 1.38$). The first power regression with $|\alpha|$ close to 3 indicates that all particle shapes are practically identical, and $\beta^*_n \sim 1$ informs the average shape angularity is close to the sphere. Therefore, this set of α and β * correctly pinpoints the near-spherical particle group. On the other hand, $|\alpha|$ of the other group has a gentler slope of -2.64. This $|\alpha| < 3$ indicates that the smaller particles have more angular which is as designed when creating the group of mixed shapes. The overall angularity is certainly higher than the first group (near-spherical) due to the mixed shapes, which is identified by the higher β^*_n value (= 1.38).

3.2 Mineral particles

A set of 60 limestone particles provided by the Florida Department of Transportation are analyzed for the evaluation of α and β *. Figure 10 shows the studied limestone particles. The A/V and V data are obtained through 3D scanning. This study adopts the Polyga C504 structured light scanner capable of obtaining high-quality 3D images [41]. The scanner is equipped with a pair of high-resolution cameras that

can capture up to 6-micron details. The companion Polyga software creates the 3D images in a standard 3D image format including OBJ and STL, from which the A/V and V data is numerically obtained. The geometric properties are presented in Table 8. Figure 11 shows the phenotypic traits of particle geometries from the power regression. The obtained α is -2.81 and β^* is 227.55 ($\beta^*_n = 2.01$). The $|\alpha| = 2.81 < 3$ indicates that there is a tendency of smaller particles being slightly more angular than larger particles. Compared to the 200 polyhedral particles in Fig. 8, the β^*_n is higher due to the overall higher angularity of the mineral particles as shown in Fig. 10.

3.3 Fragmented particles

Fragmented particles are analyzed for the evaluation of α and β^* . This study analyzes the geometric properties of 86 fragmented particles provided by Zheng et al. [42]. The particle images are shown in Fig. 12. The particles with a higher ID in the figure are smaller, and the geometric properties are summarized in Table 9 (which can be also found in Table A1 in the original article [42]). Figure 13 shows the phenotypic traits of particle geometries from the power regression. The obtained α is -2.37 and β^* is 271.90 ($\beta^*_n = 2.40$). The high β^* reflects the high angularity of the fragmented particles due to the sharp edges and corners generated by the breakage. The smaller particles (with a higher ID in the figure) are more angular than larger particles, so $|\alpha| < 3$ accurately represents the shape-size relation.

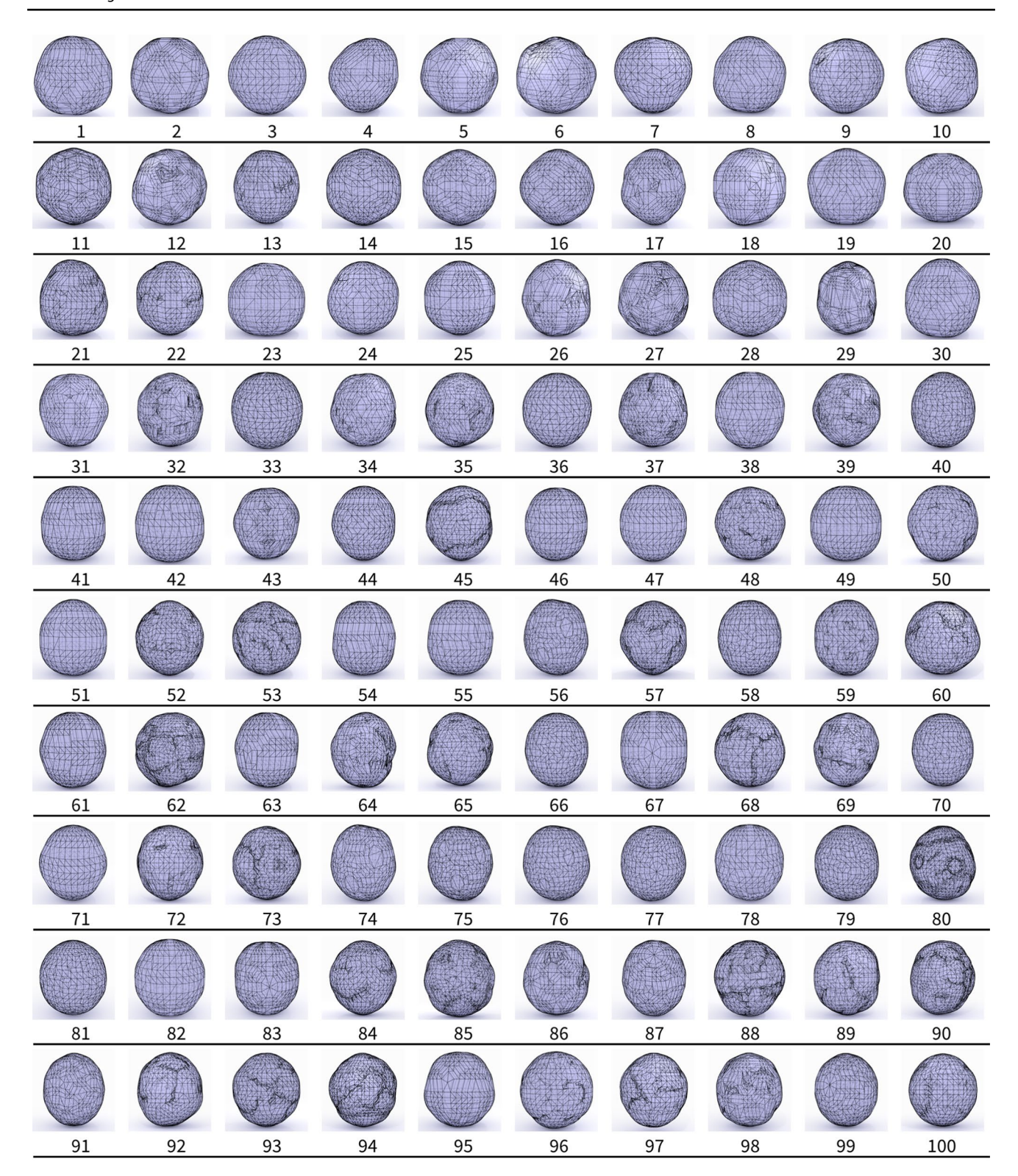
4 Characterization of individual particle geometry

4.1 Wadell's true sphericity vs. M-A-V-L

Given the A/V and V data of the particles, the phenotypic trait of a granular material (i.e., a group of particles) can be characterized by α and β^* as discussed in Sects. 2 and 3. A follow-up question then is whether it is also possible to characterize 'individual' particle shape using the A/V and V data. The answer is 'yes' by using Wadell's 'true Sphericity' [43]. Wadell proposed the 'true Sphericity' S to quantify the 3D particle shape in terms of the ratio between two surface areas. Equation (11) is the original definition by Wadell, where A is the surface area of the particle and A_s is the surface area of the reference sphere. The reference sphere is determined so that its volume V_s is equal to the volume V of the particle (i.e., $V_s = V$). The true Sphericity ranges between 0 and 1, with a value close to 1 indicating a near-spherical shape. It is worth noting Wadell also proposed 2D Sphericity and Roundness [6, 43] but which are different from the true Sphericity that evaluates the 3D shape.



79 Page 8 of 25 S. J. Lee et al.



 $\textbf{Fig. 8} \quad \text{Artificially generated 200 polyhedral particles (image reproduced from Su \ et \ al.\ [1])}$



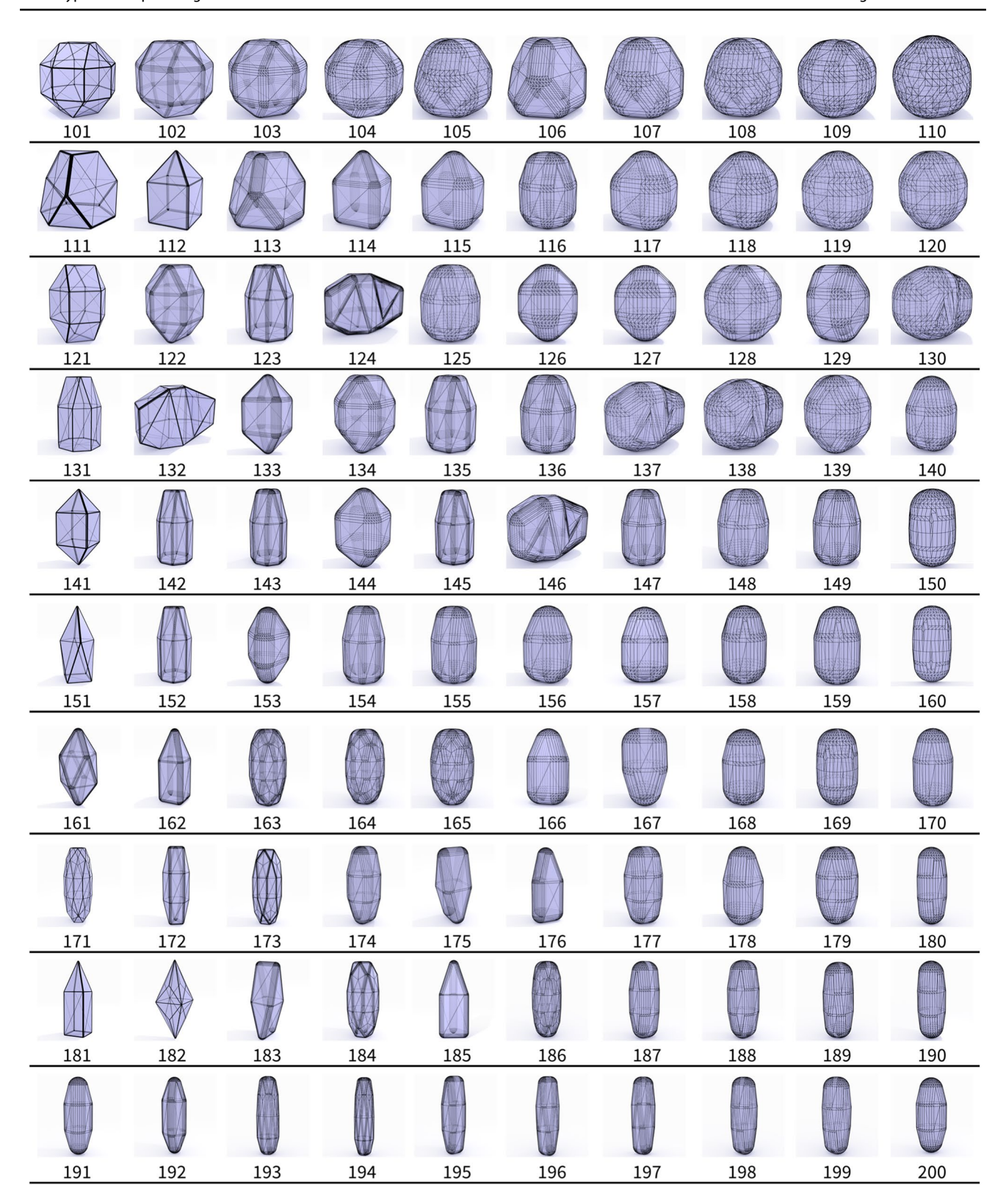


Fig. 8 (continued)



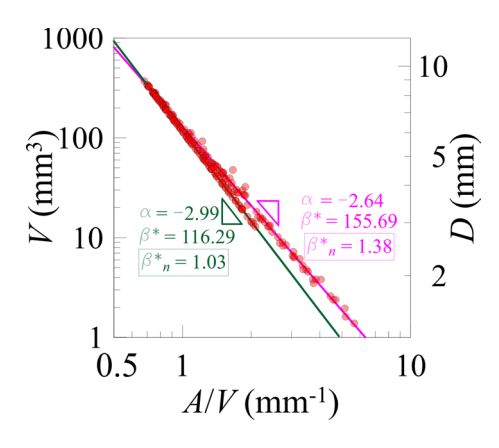


Fig. 9 Two different phenotypic traits in the 200 particles

$$S = A_s / A \tag{11}$$

The research community has used the original definition presented by Eq. (11) nearly for a century without realizing (or at least not referencing) that S can be re-formulated to define the shape as a function of surface area A, volume V, and size D. To be more specific, the inverse of true Sphericity S^{-1} is equal to $A/V \times D/6$ as shown in Eq. (12) where D is the diameter of reference sphere having the same volume as the particle. Therefore, the individual particle shape can be estimated in terms of the true Sphericity for any A/V and

V data, because D can be analytically obtained from V using Eq. (7).

The derivation of the relation is straightforward: A_s can be expressed in terms of V and D as in Eq. (13) since $V = V_s$. Then, substituting Eq. (13) for A_s in Eq. (11) results in Eq. (12). Figure 14 shows examples of five different shapes with their corresponding A, V, and D values. Since S^{-1} is the inverse of S, the lowest possible value is 1 for the sphere (Fig. 14a) which increases with angularity: The cube (Fig. 14b) has the higher S^{-1} value (=1.24) due to the higher angularity, and the great stellated dodecahedron (Fig. 14e) has the highest S^{-1} value (=2.73) due to the very high angularity.

$$1/S = S^{-1} = A/V \times D/6 \tag{12}$$

$$A_s = 4 \times \pi \times (D/2)^2 = V_s \times 6/D = V \times 6/D \tag{13}$$

However, there is a limitation to using the true Sphericity as a sole 3D particle shape index, because the particle shape can be better characterized with elongation and angularity [31, 35]. The particle elongation is concerned about the overall form that is defined at the particle's diameter scale O(d), e.g., sphere vs. ellipsoid. On the other hand, the angularity is related to the corner sharpness defined at a smaller length scale by an order of magnitude O(d/10), e.g., sphere vs. cube [6, 44]. Since the true Sphericity lacks the information about particle elongation, different shapes may have



Fig. 10 Limestone particles analyzed in this study



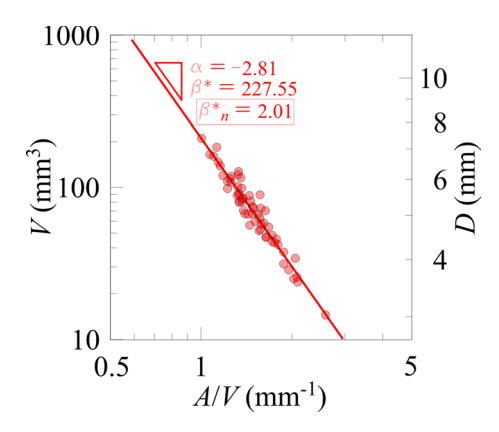
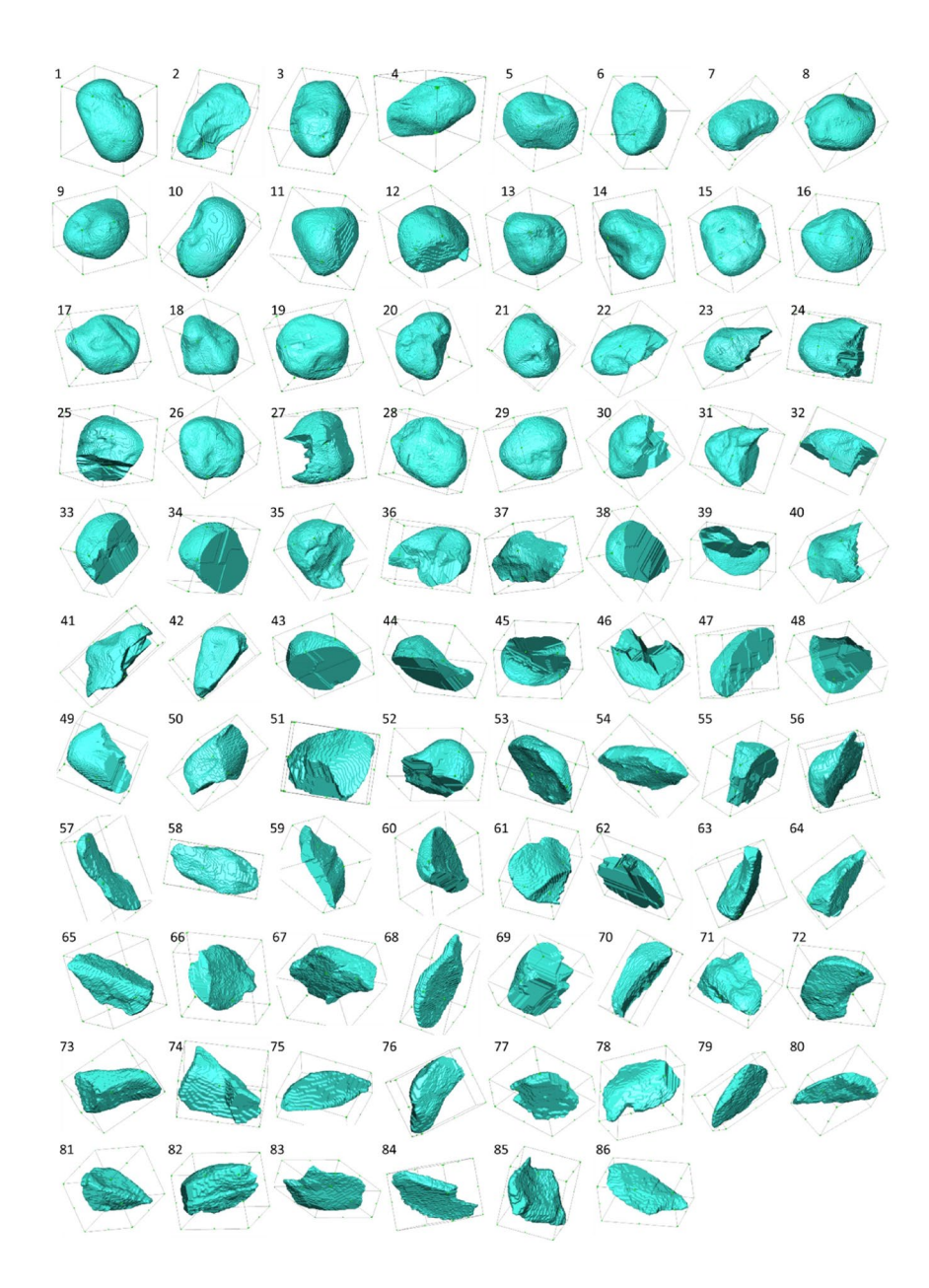


Fig. 11 Phenotypic trait of the limestone particles

a same S^{-1} value such as the pentagon pyramid (Fig. 14c) and the elongated tetrahedron (Fig. 14d). Therefore, additional information regarding elongation is needed to better characterize the shape. The true Sphericity has an inherent limitation in properly evaluating the elongation because the size D in Eq. (12) is not the actual particle size but the size of the reference sphere having the same volume as the particle. Therefore, all example particles in Fig. 14 have the same size D regardless of the actual elongation because all particles have the same unit volume. Since the size D can be computed from V per Eq. (7), the D is also a redundant information, so which can be replaced with more meaningful size information to account for the elongation.

Fig. 12 Fragmented particles analyzed in this study (Image from Zheng et al. [42]); This figure is reused with the written permission from Elsevier





79 Page 12 of 25 S. J. Lee et al.

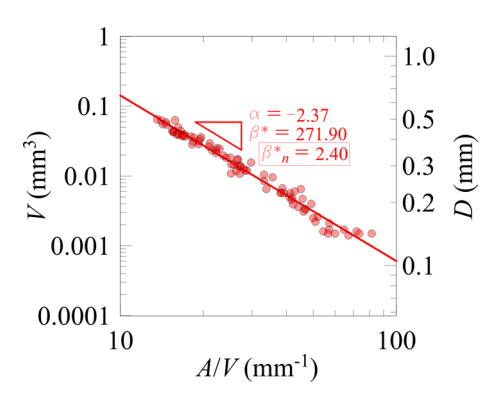


Fig. 13 Phenotypic trait of the fragmented particles

Therefore, we propose to use M as the second index that is defined with the additional size information L as in Eq. (14). The shape index M was originally proposed by Su et al. [1] to quantify the particle shape as a function of surface area, volume, and size, then without knowing that Wadell's true sphericity could be similarly formulated. Compared to Eq. (12), the shape index M considers L instead of D. The size L is the actual particle size evaluated by the circumdiameter (i.e., diameter of particle's circumsphere) which therefore considers the length to the farthest corner of the particle. A schematic comparison of D and L is shown in Fig. 14c and d (where D represents the diameter of reference sphere in Fig. 14a). Since L is always greater than or equal to D, the M values obtained for the five shapes in Fig. 14 are also greater than or equal to S^{-1} . Therefore, as in Eq. (15),

the M/S^{-1} ratio (simply $M \times S$) is the ratio of L/D which informs the particle elongation. It is worth noting the M/S^{-1} ratio is the elongation compared to sphere having the same volume as the particle (i.e., based on L/D), which therefore is different from the conventional measure based on the aspect ratio that compares the longest and smallest dimensions of the particle.

$$M = A/V \times L/6 \tag{14}$$

$$M/S^{-1}(=M\times S) = L/D \tag{15}$$

The elongated tetrahedron (Fig. 14d) has the higher M/S^{-1} value than the pentagon pyramid (Fig. 14c) because of the elongation. The great stellated dodecahedron (Fig. 14e) has the highest values of M and S^{-1} among the five shapes due to the very high angularity, but the elongated tetrahedron (Fig. 14d) has the highest value of M/S^{-1} due to the elongation.

If we could compute M using Eq. (14), it means we could also get L/D because D can be directly computed from V using Eq. (7). In that sense, M contains the S^{-1} information. The S^{-1} and M values of the example particles in Sect. 3.1 and 3.2 are summarized in Tables 7 and 8. The A/V and V data may be presented as a 3D plot with the additional information L, on which a power regression can be also obtained. For example, Fig. 15 clearly reveals the phenotypic traits of the 200 polyhedral particles (in Sect. 3.1) as a 3D plot.

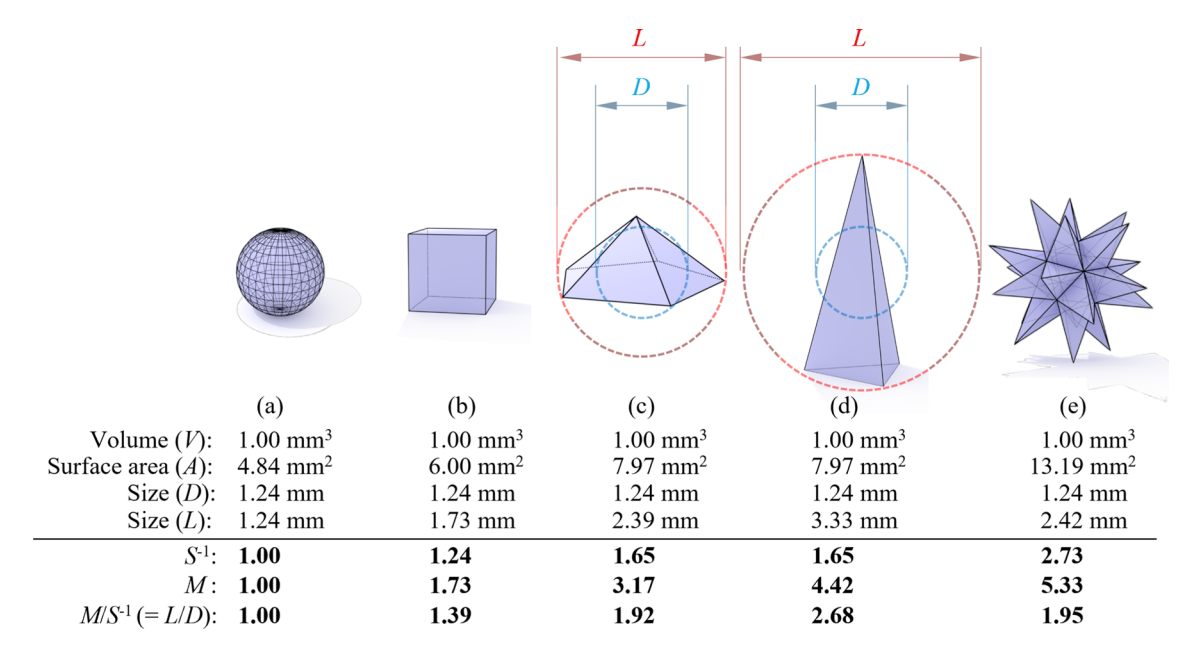


Fig. 14 Particle shape characterization in terms of surface area, volume, and size: a Sphere; b Cube; c Pentagon pyramid; d Elongated tetrahedron; and e Great stellated dodecahedron



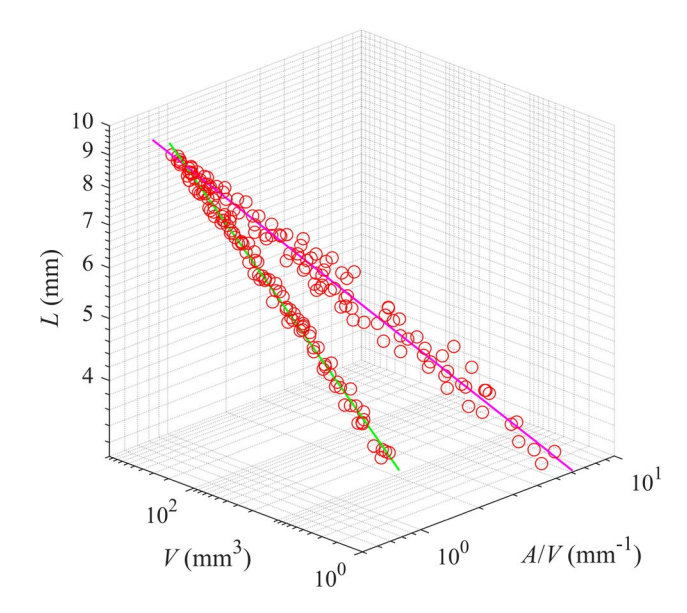


Fig. 15 Two different phenotypic traits of the 200 particles evaluated in 3D

4.2 M/S⁻¹, β_n , and shear strength

The individual particle elongation and angularity can be quantified with M/S^{-1} and β_n which are simple to use for the 3D particle shape characterization. In this section, we discuss the predictive capability of M/S^{-1} and β_n to estimate the effect of particle shape on the mechanical behavior of granular material. To this end, the experimental data reported in Murphy, Dahmen, and Jaeger [45] are utilized.

Murphy et al. [45] investigated the changes in the triaxial compression behavior by varying the particle shape and reported the corresponding shear strength (in terms of friction angle ψ) obtained per each shape. A total of 22 particle shapes were considered in their study [45] as shown in Fig. 16. The lens shape particle is made of two spherical caps with polar angle γ , and the angle ζ is the aperture of the truncated cone shape. The D/t is the diameter-to-thickness ratio, and m is the parameter to control the supercube surface, e.g., m=2 for sphere. All 22 shapes were numerically created and scaled to have the same volume of 22.5 mm³ except the 'corner' shape (shape ID: F) created by clumping three cubes that has a volume of 67.5 mm³. The geometric properties of the 22 particles are summarized in Table 10 in Appendix, where the computed M/S^{-1} and β_n values are also presented for each shape. The particles are 3D printed and packed to develop the 10-cm high and 5-cm diameter cylindrical packings, thereby 22 packed specimens are made with each particle shape. Therefore, all particles in each specimen have an identical shape, thus $\beta^*_n = \beta_n$. Around 5000 particles were used to develop each specimen except the 'corner' particles requiring a third due to the different volume. The triaxial compression tests were conducted on the specimens with 20 kPa of cell confining pressure. Murphy et al. [45] then showed an overall positive correlation between the friction angle ψ and S^{-1} , i.e., a higher S^{-1} tends to result in a higher ψ .

We concur with the findings in the paper. However, the data could be better interpreted because S^{-1} considered in their study is a single-parameter shape index that has the limitation in evaluating the shape elongation as discussed in Sect. 4.1. For example, both 'triangular bipyramid' and 'divot cube' (shape ID: C and E) have similar S^{-1} values (which are 1.408 and 1.420, respectively; see Table 10) although the 'triangular bipyramid' has a more elongated shape than the 'divot cube'. Murphy et al. [45] observed a considerably higher friction angle ψ in the 'triangular bipyramid' testing than in the 'divot cube' (by more than 5 degrees), but which was not properly explained with S^{-1} alone. In that sense, M/S^{-1} and β_n can be a useful set of alternatives to better understand the relation between the particle shape and the mechanical behavior. The color contour in Fig. 16 shows a linear regression of the friction angles ψ reported in [45] and its correlation with the M/S^{-1} and β_n data of the 22 particle shapes. The Matlab fit function is used for the regression. The range of ψ is shown on the color bar in the figure. The shape IDs (A to V in the list) are alphabetically sorted from the farthest to the nearest to the 'sphere' with $(M/S^{-1}, \beta_n) = (1, 1)$. For example, the M/S^{-1} and β_n of 'tetrahedron' are 2.013 and 3.308, respectively, which is the farthest from the 'sphere' thus named A; the 'disk (D/t = 4.5)' is the next, so which is B, and so on. Figure 16 clearly shows that ψ tends to be higher as the shape deviates further from the sphere. The M/S^{-1} of aforementioned 'triangular bipyramid' is 2.131 (ID: C), while that of 'divot cube' is 1.483 (ID: E), which reflects the different shape elongations that resulted in the different friction angles while the angularities evaluated in terms of β_n are relatively comparable. This shows the effect of particle geometries can be properly estimated with M/S^{-1} and β_n .

5 Concluding remarks

This paper provides a new perspective on how the phenotypic trait can be discovered in the particle geometries, demonstrating the particle surface-area-to-volume ratio (A/V) and the particle volume (V) are the key information. The proposed approach using A/V and V provides a unified method that can comprehensively characterize the particle geometry at multiple scales from (i) granular material to (ii) single particle.

(i) Phenotypic trait of a granular material—The relation between A/V and V data of a granular material can be



79 Page 14 of 25 S. J. Lee et al.

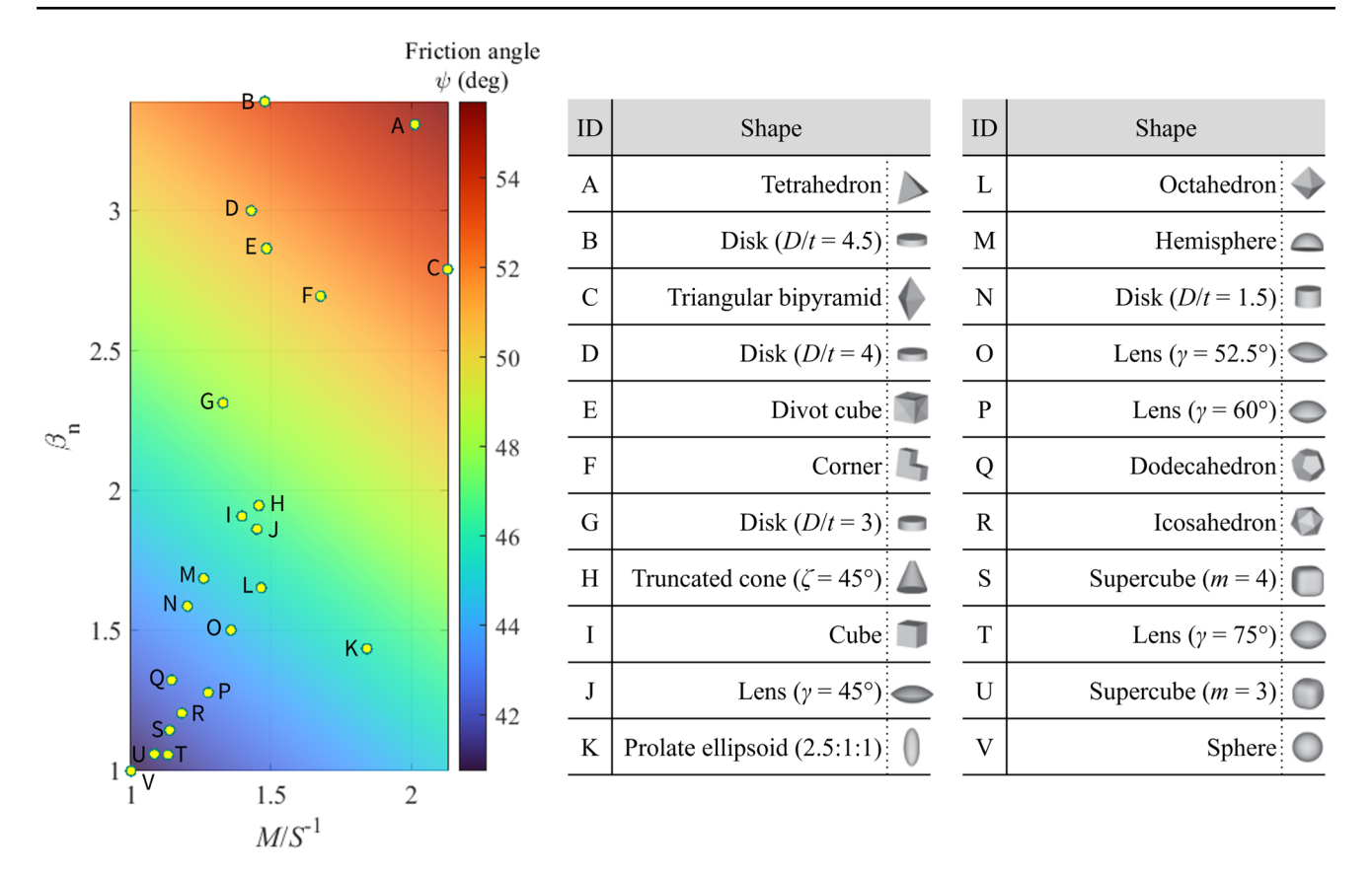


Fig. 16 Geometry-dependent shear strengths (friction angles) of packed particles; The images of the 22 particles in the table (shape ID: A to V) are reproduced from Murphy, Dahmen, and Jaeger [45]

approximated by a 'power-law' that can uncover the 'phenotypic trait' of the particle geometries. This phenotypic trait is realized as a linear plot in a log-log space, where the power value α (slope) represents the relation between particle shape and size, while the intercept term β^* (evaluated by the constrained analysis for $\alpha=-3$) informs the 'average' shape angularity. In addition, particle volume, surface area, and size can be considered together in this A/V and V space, allowing for comprehensive particle geometry characterization of a granular material.

(ii) Single particle geometry—The A/V and V information can be also used for single particle geometry quantification. The 3D shape of individual particle can be characterized using the A/V and V values in terms of Wadell's true Sphericity S. The concept is linked to another shape index M that extends the concept of Wadell's true Sphericity with additional size information L. This paper finds M/S^{-1} (simply $M \times S$) provides the useful information about particle elongation. The individual particle angularity can be obtained by β (just as β^* informs the average shape angularity in a granular material). Therefore, a complete set of single particle geometry information (i.e., elongation and angularity) can be obtained using A, V, and L. Furthermore, this approach comprehensively

describes how the particle shape is related to surface area (A), volume (V), and size (D or L) which is a powerful feature compared to the conventional methods (e.g., commonly used 2D sphericity and roundness) that separately describe the shape without referring to the surface area, volume, and size information.

The A/V ratio is also known in the granular materials research community as the 'specific surface area per unit volume', which is considered an important particle-scale property that affects the physical phenomena of solids. The proposed approach directly defines the particle shape in terms of A/V, which therefore will allow us to better interpret the associated physical phenomena such as modulus, strength, permeability, transport processes, etc.

The findings in this paper will also allow for more effective DEM particle geometry modeling. In general, there are too many particle shapes that exist in a naturally occurring granular material. Considering not all shapes can be modeled for the DEM analysis, some representative shapes need to be somehow identified for the particle modeling. However, it has been always unclear to determine what shapes to model. Furthermore, the



selection of such shapes has been somewhat subjective in the DEM research community. These questions may be better addressed by using the proposed approach in this paper. Also, using the identified phenotypic trait, a set of synthetic particles having the same geometric features can be systematically produced for the DEM analysis.

The findings in this study can be extended to identify the phenotypic trait of any granular materials in general, e.g., coffee beans, cereal grains, chemical powders, etc. The granular materials affect our daily lives in every different way considering it is the second-most manipulated material next to water [46]. This study will help to systematically address the particle geometry and better understand the complex behavior of the granular materials.

Appendix

See Tables 1, 2, 3, 4, 5, 6, 7, 8, 9 and 10.

Table 1 Geometric properties of Group 1 (Spheres only)

		1	1 \ 1	3,	
Group 1	D (mm)	$V (\text{mm}^3)$	$A \text{ (mm}^2)$	$A/V (\mathrm{mm}^{-1})$	$\log(\beta)^{\dagger}$
Sphere	0.322	0.018	0.327	18.611	2.053
	0.403	0.034	0.510	14.888	2.053
	0.484	0.059	0.735	12.407	2.053
	0.564	0.094	1.000	10.635	2.053
	0.645	0.140	1.306	9.305	2.053
	0.725	0.200	1.653	8.271	2.053
	0.806	0.274	2.041	7.444	2.053
	1.612	2.193	8.163	3.722	2.053
	2.418	7.402	18.368	2.481	2.053
	3.224	17.546	32.654	1.861	2.053
	4.030	34.269	51.022	1.489	2.053
	4.836	59.218	73.471	1.241	2.053
	5.642	94.035	100.003	1.063	2.053
	6.448	140.368	130.616	0.931	2.053
	7.254	199.859	165.311	0.827	2.053
				$\beta^* =$	113.09
				$\beta^*_n =$	1.00

 $^{^{\}dagger}\log(\beta) = \log(V) + 3 \times \log(A/V)$

 Table 2 Geometric properties of Group 2 (Cubes only)

Group 2	D (mm)	$V (\mathrm{mm}^3)$	A (mm ²)	$A/V (\text{mm}^{-1})$	$\log(\beta)$
Cube	0.400	0.034	0.624	18.611	2.334
	0.500	0.065	0.974	14.888	2.334
	0.600	0.113	1.403	12.407	2.334
	0.700	0.180	1.910	10.635	2.334
	0.800	0.268	2.495	9.305	2.334
	0.900	0.382	3.157	8.271	2.334
	1.000	0.524	3.898	7.444	2.334
	2.000	4.189	15.591	3.722	2.334
	3.000	14.137	35.080	2.481	2.334
	4.000	33.510	62.364	1.861	2.334
	5.000	65.450	97.444	1.489	2.334
	6.000	113.097	140.320	1.241	2.334
	7.000	179.594	190.991	1.063	2.334
	8.000	268.083	249.458	0.931	2.334
	9.000	381.704	315.720	0.827	2.334
				$\beta^* =$	216.00
				$\beta^*_n =$	1.91

Table 3 Geometric properties of Group 3 (Tetrahedra only)

Group 3	D (mm)	$V (\mathrm{mm}^3)$	A (mm ²)	$A/V (\mathrm{mm}^{-1})$	$\log(\beta)$
Tetrahe- dron	0.480	0.058	1.080	18.611	2.573
	0.600	0.113	1.688	14.888	2.573
	0.721	0.196	2.430	12.407	2.573
	0.841	0.311	3.308	10.635	2.573
	0.961	0.464	4.321	9.305	2.573
	1.081	0.661	5.468	8.271	2.573
	1.201	0.907	6.751	7.444	2.573
	2.402	7.255	27.005	3.722	2.573
	3.603	24.486	60.760	2.481	2.573
	4.804	58.042	108.018	1.861	2.573
	6.005	113.362	168.779	1.489	2.573
	7.206	195.890	243.041	1.241	2.573
	8.407	311.067	330.806	1.063	2.573
	9.607	464.333	432.073	0.931	2.573
	10.808	661.130	546.843	0.827	2.573
				$\beta^* =$	374.12
				$\beta^*_n =$	3.31



79 Page 16 of 25 S. J. Lee et al.

Table 4 Geometric properties of Group A and B in Figs. 4 and 5

	D (mm)	$V (\text{mm}^3)$	$A \text{ (mm}^2)$	$A/V (\mathrm{mm}^{-1})$	$\log(\beta)$
Group A					
Sphere	2.418	7.402	18.368	2.481	2.053
Cube	4.000	33.510	62.364	1.861	2.334
Tetrahedron	6.005	113.362	168.779	1.489	2.573
				$\beta^* =$	209.08
				$\beta^*_n =$	1.85
Group B					
Sphere	4.836	59.218	73.471	1.241	2.053
Cube	4.000	33.510	62.364	1.861	2.334
Tetrahedron	3.603	24.486	60.760	2.481	2.573
				$\beta^* =$	209.08
				$\beta^*_n =$	1.85
Group B	D (cm)	$V(\text{cm}^3)$	A (cm ²)	$A/V (\text{cm}^{-1})$	$\log(\beta)$
Sphere	0.484	0.059	0.735	12.407	2.053
Cube	0.400	0.034	0.624	18.611	2.334
Tetrahe- dron	0.360	0.024	0.608	24.814	2.573
				$\beta^* =$	209.08
				$\beta^*_n =$	1.85

Table 5 Geometric properties of particles in Fig. 6

	$D (\mathrm{mm})$	$V (\text{mm}^3)$	$A \text{ (mm}^2)$	$A/V (\mathrm{mm}^{-1})$	$\log(\beta)$
Figure 6a					
Sphere	1.241	1.000	4.836	4.836	2.053
Cube	1.241	1.000	6.000	6.000	2.334
Tetrahedron	1.241	1.000	7.206	7.206	2.573
				$\beta^* =$	209.08
				$\beta^*_n =$	1.85
Figure 6b					
Sphere	1.241	1.000	4.836	4.836	2.053
Cube	1.241	1.000	6.000	6.000	2.334
ET^{\dagger}	1.241	1.000	7.972	7.972	2.705
				$\beta^*=$	231.31
				$\beta^*_n =$	2.05
Figure 6c					
Sphere 1	1.241	1.000	4.836	4.836	2.053
Sphere 2	1.241	1.000	4.836	4.836	2.053
Cube	1.241	1.000	6.000	6.000	2.334
Tetrahedron	1.241	1.000	7.206	7.206	2.573
				$\beta^* =$	179.31
				$\beta^*_n =$	1.59
Figure 6d					
Sphere 1	1.241	1.000	4.836	4.836	2.053
Sphere 2	1.241	1.000	4.836	4.836	2.053
Sphere 100	1.241	1.000	4.836	4.836	2.053
Cube	1.241	1.000	6.000	6.000	2.334
Tetrahedron	1.241	1.000	7.206	7.206	2.573
				$\beta^* =$	115.16
				$\beta^*_n =$	1.02

 $^{^{\}dagger}\mathrm{ET}\mathrm{:}$ Elongated Tetrahedron

Table 6 Geometric properties of a variation to Fig. 6b

	D (mm)	$V (\mathrm{mm}^3)$	A (mm ²)	$A/V (\mathrm{mm}^{-1})$	$\log(\beta)$
Sphere	11.664	830.985	427.444	0.514	2.053
Cube	5.309	78.362	109.872	1.402	2.334
ET^{\dagger}	6.204	125.000	199.293	1.594	2.705
				$\beta^* =$	231.31
				$\beta^*_n =$	2.05

 $[\]dagger ET:$ Elongated Tetrahedron (the length of long edges is 16 each, and the base edge length is 7.5 each.)



Table 7 Geometric properties of 200 polyhedral particles

ID	D (mm)	$V (\text{mm}^3)$	A (mm ²)	$A/V (\mathrm{mm}^{-1})$	$\log(\beta)$	L (mm)	S^{-1}	M
1	8.550	327.290	232.718	0.711	2.071	8.984	1.013	1.065
2	8.487	320.079	228.506	0.714	2.066	8.876	1.010	1.056
3	8.510	322.706	228.806	0.709	2.061	8.830	1.006	1.043
4	8.069	275.090	207.197	0.753	2.070	8.780	1.013	1.102
5	8.166	285.101	211.747	0.743	2.067	8.726	1.011	1.080
6	8.148	283.212	210.673	0.744	2.067	8.612	1.010	1.068
7	8.035	271.628	204.718	0.754	2.066	8.604	1.009	1.081
8	8.037	271.849	204.696	0.753	2.065	8.565	1.009	1.075
9	8.198	288.523	212.411	0.736	2.061	8.501	1.006	1.043
10	7.922	260.339	199.146	0.765	2.066	8.435	1.010	1.075
11	8.115	279.769	208.054	0.744	2.061	8.370	1.006	1.037
12	8.152	283.699	211.156	0.744	2.068	8.365	1.011	1.038
13	7.512	221.988	178.867	0.806	2.065	8.262	1.009	1.109
14	7.883	256.509	196.280	0.765	2.060	8.130	1.005	1.037
15	7.751	243.775	189.881	0.779	2.061	8.020	1.006	1.041
16	7.596	229.494	182.857	0.797	2.065	8.020	1.009	1.065
17	7.109	188.155	161.096	0.856	2.072	8.010	1.015	1.143
18	7.495	220.458	178.369	0.809	2.067	7.996	1.011	1.078
19	7.682	237.395	186.920	0.787	2.064	7.979	1.008	1.047
20	7.397	211.951	173.829	0.820	2.068	7.870	1.011	1.076
21	7.209	196.139	165.054	0.842	2.068	7.843	1.011	1.100
22	7.147	191.186	161.606	0.845	2.062	7.635	1.007	1.076
23	7.349	207.783	171.059	0.823	2.064	7.601	1.008	1.043
24	7.278	201.886	167.276	0.829	2.060	7.539	1.005	1.043
25	7.173	193.269		0.843		7.499		1.053
	6.793	164.157	162.905 147.046	0.896	2.063		1.008 1.014	1.110
26 27		169.398			2.072	7.436	1.014	
	6.865		150.063	0.886	2.071	7.383		1.090
28	7.135	190.218	160.938	0.846	2.061	7.384	1.006	1.041
29	6.594	150.141	138.827	0.925	2.074	7.379	1.016	1.137
30	6.841	167.654	148.309	0.885	2.065	7.291	1.009	1.075
31	6.793	164.120	146.524	0.893	2.067	7.280	1.011	1.083
32	6.603	150.721	138.425	0.918	2.067	7.267	1.011	1.112
33	6.891	171.323	149.775	0.874	2.059	7.224	1.004	1.053
34	6.686	156.489	141.858	0.907	2.067	7.161	1.010	1.082
35	6.549	147.044	135.700	0.923	2.063	7.033	1.007	1.082
36	6.566	148.238	136.005	0.917	2.059	6.976	1.004	1.067
37	6.476	142.207	133.139	0.936	2.067	6.967	1.011	1.087
38	6.419	138.474	130.285	0.941	2.062	6.871	1.007	1.077
39	6.219	125.946	122.711	0.974	2.066	6.772	1.010	1.100
40	5.995	112.798	113.789	1.009	2.064	6.740	1.008	1.133
41	6.223	126.178	122.993	0.975	2.068	6.741	1.011	1.095
42	6.309	131.495	126.011	0.958	2.063	6.718	1.008	1.073
43	6.177	123.382	121.169	0.982	2.068	6.717	1.011	1.100
44	5.815	102.934	107.128	1.041	2.065	6.544	1.009	1.135
45	6.067	116.915	116.542	0.997	2.064	6.527	1.008	1.084
46	5.781	101.145	105.924	1.047	2.065	6.345	1.009	1.107
47	5.711	97.509	103.161	1.058	2.062	6.314	1.007	1.113
48	5.978	111.839	113.060	1.011	2.063	6.296	1.007	1.061
49	5.816	102.983	106.821	1.037	2.060	6.050	1.005	1.046
50	5.681	96.024	102.063	1.063	2.062	6.026	1.006	1.067
51	5.573	90.624	98.316	1.085	2.063	6.007	1.008	1.086



 Table 7 (continued)

ID	D (mm)	$V (\text{mm}^3)$	$A \text{ (mm}^2)$	$A/V (\mathrm{mm}^{-1})$	$\log(\beta)$	L (mm)	S^{-1}	
52	5.485	86.386	95.043	1.100	2.061	5.954	1.006	1.092
53	5.640	93.912	100.374	1.069	2.059	5.935	1.005	1.057
54	5.404	82.631	93.016	1.126	2.071	5.931	1.014	1.113
55	5.504	87.290	96.052	1.100	2.066	5.915	1.009	1.085
56	5.217	74.343	86.582	1.165	2.070	5.861	1.013	1.138
57	5.209	73.993	86.166	1.165	2.068	5.708	1.011	1.108
58	5.103	69.564	82.545	1.187	2.065	5.695	1.009	1.126
59	5.022	66.328	80.169	1.209	2.069	5.592	1.012	1.127
60	5.287	77.360	88.307	1.142	2.061	5.484	1.006	1.043
61	4.927	62.641	77.038	1.230	2.066	5.386	1.010	1.104
62	4.943	63.249	77.885	1.231	2.072	5.343	1.015	1.097
63	4.847	59.640	74.805	1.254	2.071	5.345	1.013	1.117
64	4.749	56.097	71.986	1.283	2.074	5.265	1.016	1.126
65	4.818	58.545	73.572	1.257	2.065	5.199	1.009	1.089
66	4.643	52.423	68.262	1.302	2.064	5.170	1.008	1.122
67	4.774	56.974	72.619	1.275	2.072	5.146	1.014	1.093
68	4.882	60.920	75.246	1.235	2.060	5.113	1.005	1.053
69	4.533	48.764	65.490	1.343	2.072	5.095	1.015	1.140
70	4.510	48.031	64.445	1.342	2.065	5.058	1.009	1.131
71	4.529	48.640	64.995	1.336	2.065	5.034	1.009	1.121
72	4.531	48.700	65.033	1.335	2.064	4.983	1.008	1.109
73	4.595	50.783	66.997	1.319	2.067	4.967	1.010	1.092
74	4.373	43.794	60.958	1.392	2.072	4.939	1.015	1.146
75	4.380	44.003	60.977	1.386	2.069	4.878	1.012	1.127
76	4.288	41.272	58.230	1.411	2.064	4.682	1.008	1.101
77	4.191	38.539	55.780	1.447	2.068	4.687	1.011	1.131
78	4.278	40.989	57.920	1.413	2.063	4.617	1.007	1.087
79	3.911	31.321	48.455	1.547	2.064	4.445	1.008	1.146
80	4.044	34.637	51.951	1.500	2.068	4.415	1.011	1.104
81	4.023	34.103	51.101	1.498	2.060	4.382	1.005	1.094
82	4.072	35.363	52.397	1.482	2.061	4.343	1.006	1.072
83	3.944	32.127	49.420	1.538	2.068	4.266	1.011	1.094
84	3.791	28.530	45.526	1.596	2.064	4.153	1.008	1.105
85	3.829	29.401	46.518	1.582	2.066	4.090	1.010	1.079
86	3.735	27.282	44.314	1.624	2.068	4.074	1.011	1.103
87	3.549	23.414	40.119	1.713	2.071	4.061	1.014	1.160
88	3.646	25.368	42.016	1.656	2.062	3.832	1.006	1.058
89	3.545	23.323	39.891	1.710	2.067	3.826	1.010	1.091
90	3.448	21.462	37.783	1.760	2.069	3.824	1.012	1.122
91	3.313	19.034	34.795	1.828	2.065	3.749	1.009	1.142
92	3.309	18.976	34.743	1.831	2.066	3.646	1.010	1.113
93	3.335	19.418	35.187	1.812	2.063	3.610	1.007	1.089
94	3.334	19.396	35.280	1.819	2.067	3.592	1.011	1.090
95	3.407	20.709	36.784	1.776	2.065	3.597	1.009	1.065
96	3.137	16.163	31.091	1.924	2.061	3.323	1.006	1.065
97	3.006	14.222	28.597	2.011	2.063	3.285	1.007	1.101
98	2.962	13.613	27.910	2.050	2.069	3.265	1.012	1.116
99	2.905	12.838	26.798	2.087	2.067	3.252	1.011	1.131
100	3.019	14.413	28.805	1.999	2.061	3.192	1.006	1.063
101	7.437	215.333	181.430	0.843	2.110	8.109	1.044	1.139
102	8.124	280.709	214.140	0.763	2.096	8.719	1.033	1.109



 Table 7 (continued)

ID	D (mm)	$V (\text{mm}^3)$	A (mm ²)	$A/V (\mathrm{mm}^{-1})$	$\log(\beta)$	L (mm)	S^{-1}	M
103	7.593	229.203	185.476	0.809	2.084	8.042	1.024	1.085
104	8.547	326.946	232.899	0.712	2.073	8.912	1.015	1.058
105	7.707	239.696	191.451	0.799	2.087	8.296	1.026	1.104
106	5.992	112.634	122.463	1.087	2.161	6.954	1.086	1.260
107	7.402	212.349	179.450	0.845	2.108	8.167	1.043	1.150
108	8.094	277.643	209.486	0.755	2.076	8.587	1.018	1.080
109	8.887	367.542	250.045	0.680	2.063	9.135	1.008	1.036
110	8.613	334.526	234.685	0.702	2.063	9.101	1.007	1.064
111	4.494	47.538	78.938	1.661	2.338	5.920	1.244	1.639
112	3.844	29.752	54.514	1.832	2.263	5.566	1.174	1.700
113	5.608	92.344	112.758	1.221	2.226	6.850	1.141	1.394
114	4.429	45.501	67.742	1.489	2.177	5.822	1.099	1.445
115	5.622	93.016	105.239	1.131	2.129	6.915	1.060	1.304
116	6.865	169.370	154.096	0.910	2.106	8.168	1.041	1.239
117	7.127	189.581	164.399	0.867	2.092	8.201	1.030	1.185
118	7.429	214.690	176.627	0.823	2.078	8.264	1.019	1.133
119	7.701	239.175	188.767	0.789	2.070	8.395	1.013	1.104
120	7.701	250.261	194.500	0.777	2.070	8.623	1.013	1.117
121	4.619		73.095			6.178	1.013	1.458
121	5.815	51.605 102.953	112.975	1.416 1.097	2.166	7.395		
					2.134		1.063	1.352
123	4.414	45.042	68.136	1.513	2.193	6.049	1.113	1.525
124	3.705	26.632	49.764	1.869	2.240	5.119	1.154	1.594
125	6.525	145.441	137.900	0.948	2.093	7.563	1.031	1.195
126	5.518	87.994	98.683	1.121	2.094	6.853	1.031	1.281
127	6.333	133.011	128.502	0.966	2.079	7.496	1.020	1.207
128	8.651	338.957	237.502	0.701	2.067	8.941	1.010	1.044
129	6.778	163.018	148.063	0.908	2.087	7.851	1.026	1.188
130	7.462	217.531	179.324	0.824	2.086	8.458	1.025	1.162
131	3.717	26.885	49.693	1.848	2.230	5.343	1.145	1.646
132	3.944	32.129	60.506	1.883	2.332	5.886	1.238	1.848
133	3.779	28.258	49.239	1.742	2.175	5.566	1.097	1.617
134	6.440	139.842	136.088	0.973	2.110	7.850	1.045	1.273
135	5.277	76.954	95.094	1.236	2.162	6.918	1.087	1.425
136	5.987	112.388	119.050	1.059	2.126	7.398	1.057	1.306
137	5.923	108.777	116.311	1.069	2.124	7.171	1.055	1.278
138	6.913	172.970	155.490	0.899	2.099	8.041	1.036	1.205
139	7.553	225.597	182.337	0.808	2.076	8.493	1.017	1.144
140	6.159	122.314	124.135	1.015	2.107	7.787	1.042	1.317
141	3.699	26.491	50.013	1.888	2.251	6.082	1.164	1.914
142	2.911	12.912	30.993	2.400	2.252	4.602	1.164	1.841
143	3.260	18.141	38.324	2.113	2.233	5.083	1.148	1.790
144	4.718	54.990	74.190	1.349	2.130	6.404	1.061	1.440
145	4.222	39.403	63.365	1.608	2.214	6.307	1.132	1.690
146	4.383	44.077	66.467	1.508	2.179	5.695	1.101	1.431
147	4.592	50.702	72.311	1.426	2.168	6.339	1.092	1.507
148	5.025	66.423	83.552	1.258	2.121	6.336	1.053	1.328
149	4.963	64.001	82.663	1.292	2.140	6.499	1.068	1.399
150	4.599	50.934	69.989	1.374	2.121	6.146	1.053	1.408
151	2.399	7.230	22.125	3.060	2.316	4.536	1.224	2.313
152	2.935	13.243	32.024	2.418	2.272	4.861	1.183	1.959
153	3.863	30.188	52.024	1.726	2.191	6.082	1.111	1.749
100	2.002	20.100	52.07	1.,20	2.1/1	0.002	1.111	I., T.



 Table 7 (continued)

ID	D (mm)	$V (\mathrm{mm}^3)$	A (mm ²)	$A/V (\mathrm{mm}^{-1})$	$\log(\beta)$	L (mm)	S^{-1}	М
154	3.776	28.180	49.453	1.755	2.183	5.408	1.104	1.582
155	4.260	40.472	61.487	1.519	2.152	5.762	1.079	1.459
156	5.431	83.874	97.987	1.168	2.126	7.205	1.057	1.403
157	4.765	56.635	76.086	1.343	2.138	6.498	1.067	1.455
158	5.039	66.989	84.967	1.268	2.136	6.952	1.065	1.470
159	5.176	72.588	88.778	1.223	2.123	6.919	1.055	1.410
160	4.666	53.201	74.190	1.395	2.159	6.855	1.085	1.593
161	3.064	15.063	33.363	2.215	2.214	5.407	1.131	1.996
162	2.089	4.773	16.676	3.494	2.309	3.802	1.216	2.214
163	4.066	35.201	57.898	1.645	2.195	6.408	1.115	1.757
164	4.377	43.895	65.607	1.495	2.166	6.497	1.090	1.618
165	4.039	34.501	55.010	1.594	2.146	5.729	1.073	1.522
166	4.481	47.109	68.489	1.454	2.161	6.402	1.086	1.551
167	4.209	39.047	59.740	1.530	2.146	5.826	1.073	1.486
168	3.822	29.239	49.233	1.684	2.145	5.405	1.073	1.517
169	4.702	54.446	74.589	1.370	2.146	6.697	1.074	1.529
170	4.192	38.581	59.936	1.554	2.160	6.146	1.085	1.591
171	2.160	5.276	17.737	3.362	2.302	4.116	1.210	2.306
172	1.705	2.597	11.555	4.450	2.359	3.574	1.265	2.651
173	2.583	9.023	24.742	2.742	2.270	4.668	1.181	2.133
174	3.126	16.001	35.081	2.192	2.227	5.246	1.142	1.917
175	2.525	8.434	23.937	2.838	2.285	4.444	1.195	2.102
176	2.312	6.469	19.989	3.090	2.281	4.055	1.191	2.088
177	3.109	15.734	33.572	2.134	2.184	4.796	1.106	1.706
178	3.436	21.237	40.904	1.926	2.181	5.117	1.103	1.643
179	3.966	32.661	53.479	1.637	2.156	5.762	1.082	1.572
180	2.914	12.959	30.727	2.371	2.237	5.182	1.152	2.048
181	1.549	1.947	10.031	5.151	2.425	3.255	1.330	2.794
182	1.884	3.501	13.132	3.751	2.267	4.057	1.178	2.537
183	1.659	2.389	11.202	4.689	2.392	3.349	1.296	2.618
184	3.007	14.242	32.749	2.299	2.238	5.147	1.153	1.972
185	1.936	3.797	15.359	4.045	2.400	3.963	1.305	2.672
186	2.684	10.122	26.494	2.618	2.259	4.862	1.171	2.121
187	3.088	15.421	34.598	2.244	2.241	5.379	1.155	2.011
188	2.792	11.399	28.206	2.474	2.237	4.827	1.152	1.991
189	2.513	8.308	22.889	2.755	2.240	4.377	1.154	2.010
190	2.294	6.324	19.457	3.077	2.265	4.314	1.176	2.212
191	2.095	4.814	16.292	3.384	2.271	4.090	1.182	2.307
192	2.056	4.550	16.156	3.551	2.309	4.379	1.217	2.591
193	1.454	1.609	8.334	5.180	2.350	3.125	1.255	2.698
194	1.383	1.384	7.839	5.663	2.400	3.252	1.305	3.069
195	1.940	3.825	14.705	3.845	2.337	4.028	1.243	2.581
196	1.658	2.386	10.920	4.576	2.359	3.607	1.245	2.751
190	2.270	6.128	20.030	3.269	2.339	4.695	1.203	2.751
198	1.936	3.797	14.148	3.726	2.293	3.738	1.202	2.338
199	2.327	6.596	19.988	3.030	2.264	4.248	1.175	2.321
200	2.566	8.845	23.615	2.670	2.204	4.248		2.143
∠00	2.300	0.843	25.013	2.070	2.220	4.5/1	1.142	2.034



79

 Table 8 Geometric properties
 of 60 Florida limestone particles

ID	D (mm)	V (mm ³)	A (mm ²)	$A/V (\mathrm{mm}^{-1})$	$\log(\beta)$	L (mm)	S^{-1}	M
1	6.134	120.867	160.352	1.327	2.451	10.283	1.356	2.274
2	5.032	66.718	103.106	1.545	2.391	7.319	1.296	1.885
3	5.043	67.160	99.098	1.476	2.334	7.065	1.240	1.737
4	4.713	54.805	91.780	1.675	2.411	7.471	1.315	2.085
5	6.236	126.957	168.909	1.330	2.476	9.923	1.383	2.200
6	7.372	209.745	210.451	1.003	2.326	10.694	1.233	1.788
7	5.177	72.655	114.487	1.576	2.454	8.310	1.360	2.182
8	4.156	37.583	70.584	1.878	2.396	6.872	1.301	2.151
9	4.026	34.176	70.121	2.052	2.470	8.405	1.377	2.874
10	5.588	91.345	121.589	1.331	2.333	8.572	1.240	1.902
11	5.126	70.537	97.418	1.381	2.269	7.057	1.180	1.624
12	4.850	59.720	90.196	1.510	2.313	7.487	1.221	1.885
13	3.631	25.067	50.839	2.028	2.320	5.309	1.227	1.794
14	5.365	80.855	107.984	1.336	2.285	8.241	1.194	1.834
15	4.929	62.684	98.103	1.565	2.381	7.630	1.286	1.990
16	4.626	51.841	80.691	1.557	2.291	5.771	1.200	1.497
17	5.029	66.591	95.346	1.432	2.291	7.559	1.200	1.804
18	5.535	88.808	116.817	1.315	2.306	7.316	1.214	1.604
19	4.660	53.001	83.361	1.573	2.314	6.529	1.222	1.711
20	3.915	31.422	58.956	1.876	2.317	5.794	1.224	1.812
21	3.795	28.623	55.863	1.952	2.328	5.244	1.235	1.706
22	3.027	14.524	37.537	2.585	2.399	4.912	1.304	2.116
23	4.524	48.494	83.481	1.721	2.393	7.444	1.298	2.136
24	5.367	80.956	110.756	1.368	2.317	7.650	1.224	1.744
25	3.569	23.812	49.738	2.089	2.336	6.038	1.243	2.102
26	3.665	25.768	53.536	2.078	2.364	5.368	1.269	1.859
27	4.380	43.983	75.620	1.719	2.349	6.449	1.255	1.848
28	4.484	47.200	77.676	1.646	2.323	7.204	1.230	1.976
29	6.540	146.444	166.775	1.139	2.335	9.741	1.241	1.849
30	5.456	85.058	117.265	1.379	2.348	8.183	1.254	1.880
31	6.014	113.910	141.973	1.246	2.343	9.544	1.249	1.983
32	5.549	89.465	140.364	1.569	2.538	9.732	1.451	2.545
33	4.785	57.360	90.697	1.581	2.356	7.703	1.261	2.030
34	6.119	119.983	141.748	1.181	2.296	9.030	1.205	1.778
35	4.313	41.996	75.571	1.799	2.389	7.369	1.293	2.210
36	4.433	45.614	80.988	1.776	2.407	6.766	1.312	2.002
37	5.119	70.254	114.845	1.635	2.487	9.250	1.395	2.520
38	6.741	160.402	176.175	1.098	2.327	9.355	1.234	1.712
39	6.416	138.308	160.196	1.158	2.332	9.277	1.239	1.791
40	6.043	115.545	156.401	1.354	2.457	9.588	1.363	2.163
41	5.908	107.950	135.627	1.256	2.331	8.171	1.237	1.711
42	6.096	118.594	149.433	1.260	2.375	8.887	1.280	1.866
43	5.549	89.478	119.948	1.341	2.334	8.520	1.240	1.904
44	5.779	101.033	133.760	1.324	2.370	8.963	1.275	1.978
45	5.434	83.993	114.994	1.369	2.334	7.547	1.240	1.722
46	5.227	74.775	110.463	1.477	2.382	8.980	1.287	2.211
47	5.737	98.881	135.019	1.365	2.401	8.747	1.306	1.991
48	4.758	56.413	81.732	1.449	2.234	6.118	1.149	1.477
49	4.478	47.006	77.063	1.639	2.316	6.500	1.223	1.776
50	5.722	98.099	119.932	1.223	2.253	8.531	1.166	1.738
51	5.189	73.159	109.218	1.493	2.386	7.577	1.291	1.885
52	5.940	109.741	134.225	1.223	2.303	8.293	1.211	1.691
53	6.812	165.476	176.663	1.068	2.304	10.125	1.212	1.802
54	4.808	58.196	93.870	1.613	2.388	7.107	1.293	1.910
55	5.372	81.168	118.436	1.459	2.402	8.202	1.306	1.995
56	7.048	183.353	206.774	1.128	2.420	11.983	1.325	2.252



Table 8 (continued)

ID	D (mm)	$V (\mathrm{mm}^3)$	$A \text{ (mm}^2)$	$A/V (\mathrm{mm}^{-1})$	$\log(\beta)$	L (mm)	S^{-1}	М
57	5.529	88.478	127.732	1.444	2.425	8.666	1.330	2.085
58	4.354	43.219	75.688	1.751	2.366	6.662	1.271	1.945
59	5.342	79.817	107.018	1.341	2.284	8.036	1.194	1.796
60	5.042	67.102	93.675	1.396	2.261	6.214	1.173	1.446

Table 9 Geometric properties of 86 fragmented particles in Zheng et al. [42]

 Table 9 (continued)

			υ	1	C			/			
[42]						ID	D (mm)	$V (\mathrm{mm}^3)$	A (mm ²)	$A/V (\text{mm}^{-1})$	$\log(\beta)$
ID	D (mm)	V (mm ³)	A (mm ²)	$A/V (\mathrm{mm}^{-1})$	$\log(\beta)$	44	0.2990	0.0140	0.381	27.2143	2.451
1	0.4978	0.0646	0.880	13.6223	2.213	45	0.2983	0.0139	0.370	26.6187	2.419
2	0.4934	0.0629	0.993	15.7870	2.394	46	0.2969	0.0137	0.372	27.1533	2.438
3	0.4918	0.0623	0.877	14.0770	2.240	47	0.2895	0.0127	0.355	27.9528	2.443
4	0.4814	0.0584	0.856	14.6575	2.265	48	0.2840	0.0120	0.345	28.7500	2.455
5	0.4727	0.0553	0.788	14.2495	2.204	49	0.2833	0.0119	0.337	28.3193	2.432
6	0.4701	0.0544	0.800	14.7059	2.238	50	0.2825	0.0118	0.310	26.2712	2.330
7	0.4559	0.0496	0.805	16.2298	2.326	51	0.2751	0.0109	0.275	25.2294	2.243
8	0.4406	0.0448	0.690	15.4018	2.214	52	0.2742	0.0108	0.293	27.1296	2.334
9	0.4403	0.0447	0.698	15.6152	2.231	53	0.2708	0.0104	0.345	33.1731	2.579
10	0.4380	0.0440	0.729	16.5682	2.301	54	0.2637	0.0096	0.342	35.6250	2.638
11	0.4337	0.0427	0.666	15.5972	2.210	55	0.2532	0.0085	0.282	33.1765	2.492
12	0.4323	0.0423	0.660	15.6028	2.206	56	0.2339	0.0067	0.259	38.6567	2.588
13	0.4264	0.0406	0.659	16.2315	2.240	57	0.2315	0.0065	0.293	45.0769	2.775
14	0.4233	0.0397	0.646	16.2720	2.233	58	0.2315	0.0065	0.220	33.8462	2.401
15	0.4229	0.0396	0.676	17.0707	2.294	59	0.2255	0.0060	0.257	42.8333	2.673
16	0.4200	0.0388	0.625	16.1082	2.210	60	0.2229	0.0058	0.222	38.2759	2.512
17	0.4200	0.0388	0.651	16.7784	2.263	61	0.2216	0.0057	0.217	38.0702	2.498
18	0.4182	0.0383	0.650	16.9713	2.272	62	0.2216	0.0057	0.223	39.1228	2.533
19	0.4138	0.0371	0.623	16.7925	2.245	63	0.2216	0.0057	0.235	41.2281	2.601
20	0.4138	0.0371	0.668	18.0054	2.336	64	0.2122	0.0050	0.205	41.0000	2.537
21	0.4131	0.0369	0.634	17.1816	2.272	65	0.2093	0.0048	0.202	42.0833	2.554
22	0.4093	0.0359	0.705	19.6379	2.434	66	0.2078	0.0047	0.215	45.7447	2.653
23	0.4081	0.0356	0.658	18.4831	2.352	67	0.2048	0.0045	0.188	41.7778	2.516
24	0.4011	0.0338	0.658	19.4675	2.397	68	0.1969	0.0040	0.197	49.2500	2.679
25	0.3914	0.0314	0.604	19.2357	2.349	69	0.1953	0.0039	0.165	42.3077	2.470
26	0.3910	0.0313	0.576	18.4026	2.290	70	0.1902	0.0036	0.159	44.1667	2.492
27	0.3829	0.0294	0.620	21.0884	2.440	71	0.1866	0.0034	0.158	46.4706	2.533
28	0.3794	0.0286	0.550	19.2308	2.308	72	0.1847	0.0033	0.155	46.9697	2.534
29	0.3790	0.0285	0.519	18.2105	2.236	73	0.1809	0.0031	0.143	46.1290	2.483
30	0.3694	0.0264	0.555	21.0227	2.390	74	0.1706	0.0026	0.135	51.9231	2.561
31	0.3642	0.0253	0.566	22.3715	2.452	75	0.1684	0.0025	0.125	50.0000	2.495
32	0.3613	0.0247	0.565	22.8745	2.471	76	0.1614	0.0022	0.112	50.9091	2.463
33	0.3544	0.0233	0.517	22.1888	2.406	77	0.1589	0.0021	0.120	57.1429	2.593
34	0.3539	0.0232	0.500	21.5517	2.366	78	0.1481	0.0017	0.097	57.0588	2.499
35	0.3450	0.0215	0.478	22.2326	2.373	79	0.1481	0.0017	0.110	64.7059	2.663
36	0.3345	0.0196	0.463	23.6224	2.412	80	0.1451	0.0016	0.115	71.8750	2.774
37	0.3270	0.0183	0.458	25.0273	2.458	81	0.1451	0.0016	0.087	54.3750	2.410
38	0.3264	0.0182	0.440	24.1758	2.410	82	0.1420	0.0015	0.085	56.6667	2.436
39	0.3221	0.0175	0.466	26.6286	2.519	83	0.1420	0.0015	0.110	73.3333	2.772
40	0.3190	0.0170	0.452	26.5882	2.505	84	0.1420	0.0015	0.122	81.3333	2.907
41	0.3100	0.0156	0.465	29.8077	2.616	85	0.1420	0.0015	0.090	60.0000	2.511
42	0.3039	0.0147	0.371	25.2381	2.373	86	0.1388	0.0014	0.094	67.1429	2.627
43	0.3025	0.0145	0.374	25.7931	2.396						



Table 10 Geometric properties of 22 particle shapes considered in Murphy et al. [45]; The surface areas *A* are not provided in [45] but were confirmed through personal communication with the first author (Kieran A. Murphy) of the paper. The other properties are then analytically computed

ID	Shape	D (mm)	$V (\mathrm{mm}^3)$	A (mm ²)	L (mm)	S^{-1}	M/S ⁻¹	β_n
A	Tetrahedron	3.503	22.500	57.428	7.052	1.490	2.013	3.308
В	Disk (D/t=4.5)	3.503	22.500	57.902	5.175	1.502	1.477	3.390
C	Triangular bipyramid	3.503	22.500	54.266	7.463	1.408	2.131	2.791
D	Disk (D/t=4)	3.503	22.500	55.588	5.007	1.442	1.429	3.000
E	Divot cube	3.503	22.500	54.745	5.196	1.420	1.483	2.866
F	Corner	5.052	67.500	111.579	8.469	1.392	1.677	2.696
G	Disk (D/t=3)	3.503	22.500	50.985	4.652	1.323	1.328	2.315
Н	Truncated cone ($\zeta = 45^{\circ}$)	3.503	22.500	48.134	5.100	1.249	1.456	1.948
I	Cube	3.503	22.500	47.820	4.890	1.241	1.396	1.910
J	Lens $(\gamma = 45^{\circ})$	3.503	22.500	47.430	5.077	1.231	1.449	1.864
K	Prolate ellipsoid (2.5:1:1)	3.503	22.500	43.487	6.452	1.128	1.842	1.436
L	Octahedron	3.503	22.500	45.581	5.130	1.183	1.465	1.654
M	Hemisphere	3.503	22.500	45.887	4.413	1.191	1.260	1.688
N	Disk (D/t = 1.5)	3.503	22.500	44.966	4.210	1.167	1.202	1.588
O	Lens $(\gamma = 52.5^{\circ})$	3.503	22.500	44.142	4.754	1.145	1.357	1.502
P	Lens $(\gamma = 60^\circ)$	3.503	22.500	41.848	4.470	1.086	1.276	1.280
Q	Dodecahedron	3.503	22.500	42.333	4.013	1.098	1.146	1.325
R	Icosahedron	3.503	22.500	41.032	4.140	1.065	1.182	1.207
S	Supercube $(m=4)$	3.503	22.500	40.325	3.987	1.046	1.138	1.145
T	Lens $(\gamma = 75^\circ)$	3.503	22.500	39.271	3.967	1.019	1.133	1.058
U	Supercube $(m=3)$	3.503	22.500	39.303	3.796	1.020	1.084	1.060
V	Sphere	3.503	22.500	38.542	3.503	1.000	1.000	1.000

Acknowledgements This work is sponsored in part by the US National Science Foundation under the awards CMMI #1938431 and #1938285. The opinions, findings, conclusions, or recommendations expressed in this article are solely those of the authors and do not necessarily reflect the views of the funding agency. The authors would like to thank Mr. Michael Kim of the Florida Department of Transportation District Four and Six Materials Office for providing the Florida limestone construction aggregate used in this study.

Declarations

Conflict of interest The authors declare that they have no conflict of interest.

Human and animal rights This research did not involve human participants or animals.

References

- Su, Y.F., Bhattacharya, S., Lee, S.J., Lee, C.H., Shin, M.: A new interpretation of three-dimensional particle geometry: M-A-V-L. Transp. Geotech. 23, 100328 (2020). https://doi.org/10.1016/j. trgeo.2020.100328
- Yang, J., Luo, X.D.: Exploring the relationship between critical state and particle shape for granular materials. J. Mech. Phys. Solids. 84, 196–213 (2015). https://doi.org/10.1016/j.jmps.2015. 08.001
- Ashmawy, A.K., Sukumaran, B., Hoang, V.V.: Evaluating The Influence of Particle Shape on Liquefaction Behavior Using Discrete Element Modeling. In: Chung, J.S. and Prinsenberg, S. (eds.)

- Proc. 13th Int.Offshore and Polar Engeering Conf. pp. 542–549. International Society of Offshore and Polar Engineers, Honolulu, Hawaii, USA (2003)
- 4. Terzaghi, K., Peck, R.B., Mesri, G.: Soil Mechanics in Engineering Practice. Wiley, Hoboken (1996)
- Mitchell, J.K., Soga, K.: Fundamentals of Soil Behavior. Wiley, Hoboken (2005)
- Cho, G.-C., Dodds, J., Santamarina, J.C.: Particle shape effects on packing density, stiffness, and strength: natural and crushed sands. J. Geotech. Geoenviron. Eng. 132, 591–602 (2006). https://doi. org/10.1061/(ASCE)1090-0241(2006)132:5(591)
- Sutherland, C.A.M., Liu, X., Zhang, L., Chu, Y., Oldmeadow, J.A., Young, A.W.: Facial first impressions across culture: datadriven modeling of Chinese and British perceivers' unconstrained facial impressions. Personal. Soc. Psychol. Bull. 44, 521–537 (2018). https://doi.org/10.1177/0146167217744194
- 8. DeBruine, L., Jones, B.: Face Research, http://faceresearch.org/
- Alderliesten, M.: Mean particle diameters, From statistical definition to physical understanding. J. Biopharm. Stat. 15, 295–325 (2005). https://doi.org/10.1081/BIP-200048774
- Alderliesten, M.: Mean particle diameters Part VIII computer program to decompose mixtures of (truncated) lognormal particle size distributions using differential evolution to generate starting values for nonlinear least squares. Part. Part. Syst. Charact. 33, 675–697 (2016). https://doi.org/10.1002/ppsc.201600086
- Alderliesten, M.: Mean particle diameters Part VII the rosinrammler size distribution: physical and mathematical properties and relationships to moment-ratio defined mean particle diameters. Part. Part. Syst. Charact. 30, 244–257 (2013). https://doi. org/10.1002/ppsc.201200021
- Alderliesten, M.: Mean particle diameters part VI: fundamental distinction between statistics based (ISO/DIN) and physics based



- (moment-ratio) definition systems. Part. Part. Syst. Charact. 27, 7–20 (2010). https://doi.org/10.1002/ppsc.201000002
- Alderliesten, M.: Mean particle diameters part V: theoretical derivation of the proper type of mean particle diameter describing a product or process property. Part. Part. Syst. Charact. 22, 233–245 (2005). https://doi.org/10.1002/ppsc.200500987
- Alderliesten, M.: Mean particle diameters part IV: empirical selection of the proper type of mean particle diameter describing a product or material property. Part. Part. Syst. Charact. 21, 179–196 (2004). https://doi.org/10.1002/ppsc.200400917
- Alderliesten, M.: Mean particle diameters part III: an empirical evaluation of integration and summation methods for estimating mean particle diameters from histogram data. Part. Part. Syst. Charact. 19, 373–373 (2002). https://doi.org/10.1002/ppsc.20029 0000
- Alderliesten, M.: Mean particle diameters part II: standardization of nomenclature. Part. Part. Syst. Charact. 8, 237–241 (1991). https://doi.org/10.1002/ppsc.19910080143
- Alderliesten, M.: Mean particle diameters part I: evaluation of definition systems. Part. Part. Syst. Charact. 7, 233–241 (1990). https://doi.org/10.1002/ppsc.19900070138
- Alderliesten, M.: Mean particle diameters: from statistical definition to physical understanding, https://repository.tudelft.nl/islandora/object/uuid%3Adfc29462-9639-4eab-a0a9-d80569a7a311, (2008)
- Su, Y.F., Lee, S.J., Sukumaran, B.: Influence of particle morphology simplification on the simulation of granular material behavior. Granul. Matter. (2020). https://doi.org/10.1007/s10035-019-0987-2
- Lim, K.: Discrete modeling of granular media: a NURBS-based approach, http://thesis.library.caltech.edu/8734/, (2015)
- Lee, S.J.: Developments in large scale discrete element simulations with polyhedral particles, https://www.ideals.illinois.edu/handle/2142/50542, (2014)
- Lee, S.J., Hashash, Y.M.A., Wilkinson, R.A., Agui, J.H.: Simulation of Experimental Tests on the JSC-1A Lunar Soil Simulant with Polyhedral Discrete Elements. In: Earth and Space 2010. pp. 208–216. American Society of Civil Engineers, Reston, VA (2010)
- 23. Wadell, H.: Volume, shape, and roundness of quartz particles. J. Geol. 43, 250–280 (1935)
- Sukumaran, B., Ashmawy, A.K.: Quantitative characterisation of the geometry of discrete particles. Géotechnique. 51, 619–627 (2001). https://doi.org/10.1680/geot.2001.51.7.619
- Tutumluer, E., Rao, C., Stefanski, J.A.: Video Image Analysis of Aggregates. Illinois Department of Transportation, Urbana, Illinois (2000)
- Sarma, G.P., Lee, C.W., Portegys, T., Ghayoomie, V., Jacobs, T., Alicea, B., Cantarelli, M., Currie, M., Gerkin, R.C., Gingell, S., Gleeson, P., Gordon, R., Hasani, R.M., Idili, G., Khayrulin, S., Lung, D., Palyanov, A., Watts, M., Larson, S.D.: OpenWorm: overview and recent advances in integrative biological simulation of Caenorhabditis elegans. Philos. Trans. R. Soc. B Biol. Sci. 373, 20170382 (2018). https://doi.org/10.1098/rstb.2017.0382
- Kong, D., Fonseca, J.: Quantification of the morphology of shelly carbonate sands using 3D images. Géotechnique. 68, 249–261 (2018). https://doi.org/10.1680/jgeot.16.P.278
- Alshibli, K.A., Druckrey, A.M., Al-Raoush, R.I., Weiskittel, T., Lavrik, N.V.: Quantifying morphology of sands using 3D imaging. J. Mater. Civ. Eng. 27, 04014275 (2015). https://doi.org/10.1061/(ASCE)MT.1943-5533.0001246
- Zhou, B., Wang, J., Wang, H.: Three-dimensional sphericity, roundness and fractal dimension of sand particles. Géotechnique. 68, 18–30 (2018). https://doi.org/10.1680/jgeot.16.P.207

- Bullard, J.W., Garboczi, E.J.: Defining shape measures for 3D star-shaped particles: Sphericity, roundness, and dimensions. Powder Technol. 249, 241–252 (2013). https://doi.org/10.1016/j.powtec. 2013 08 015
- Zhao, B., Wang, J.: 3D quantitative shape analysis on form, roundness, and compactness with μCT. Powder Technol. 291, 262–275 (2016). https://doi.org/10.1016/j.powtec.2015.12.029
- Zheng, J., Hryciw, R.D.: Traditional soil particle sphericity, roundness and surface roughness by computational geometry. Géotechnique. 65, 494–506 (2015). https://doi.org/10.1680/geot. 14 P 192.
- Lee, C.H., Lee, S.J., Shin, M., Bhattacharya, S.: Interrelation of morphological indices and 2-D generalized regularity for coarse aggregate in cement-based materials. Constr. Build. Mater. 251, 118984 (2020). https://doi.org/10.1016/j.conbuildmat.2020.118984
- Lee, C.H., Lee, S.J., Shin, M.: Characterization of variability in 2-dimensional particle geometry via 3D structured light scanning. Transp. Geotech. 34, 100760 (2022). https://doi.org/10.1016/j. trgeo.2022.100760
- Barrett, P.J.: The shape of rock particles, a critical review. Sedimentology 27, 291–303 (1980). https://doi.org/10.1111/j.1365-3091.1980.tb01179.x
- Rodriguez, J., Edeskär, T., Knutsson, S.: Particle shape quantities and measurement techniques - a review. Electron. J. Geotech. Eng. 18, 169–198 (2013)
- Blott, S.J., Pye, K.: Particle shape: a review and new methods of characterization and classification. Sedimentology 55, 31–63 (2007). https://doi.org/10.1111/j.1365-3091.2007.00892.x
- Lee, S.J., Lee, C.H., Shin, M., Bhattacharya, S., Su, Y.F.: Influence of coarse aggregate angularity on the mechanical performance of cement-based materials. Constr. Build. Mater. 204, 184–192 (2019). https://doi.org/10.1016/j.conbuildmat.2019.01.
- Bird, R.B., Stewart, W.E., Lightfoot, E.N.: Transport Phenomena. Wiley, Hoboken (2006). ISBN: 978-0-470-11539-8. https://www.wiley.com/en-us/Transport+Phenomena%2C+Revised+2nd+Edition-p-9780470115398
- Bhattacharya, S., Subedi, S., Lee, S.J., Pradhananga, N.: Estimation of 3D sphericity by volume measurement application to coarse aggregates. Transp. Geotech. 23, 100344 (2020). https://doi.org/10.1016/j.trgeo.2020.100344
- Polyga: Polyga Compact C504, https://www.polyga.com/products/ compact-c504/
- Zheng, W., Hu, X., Tannant, D.D., Zhang, K., Xu, C.: Characterization of two- and three-dimensional morphological properties of fragmented sand grains. Eng. Geol. 263, 105358 (2019). https://doi.org/10.1016/j.enggeo.2019.105358
- Wadell, H.: Sphericity and roundness of rock particles. J. Geol. 41, 310–331 (1933)
- Jerves, A.X., Kawamoto, R.Y., Andrade, J.E.: Effects of grain morphology on critical state: a computational analysis. Acta Geotech. 11, 493–503 (2016). https://doi.org/10.1007/s11440-015-0422-8
- Murphy, K.A., Dahmen, K.A., Jaeger, H.M.: Transforming mesoscale granular plasticity through particle shape. Phys. Rev. X. 9, 11014 (2019). https://doi.org/10.1103/PhysRevX.9.011014
- Richard, P., Nicodemi, M., Delannay, R., Ribière, P., Bideau, D.: Slow relaxation and compaction of granular systems. Nat. Mater. 4, 121–128 (2005). https://doi.org/10.1038/nmat1300

Publisher's Note Springer Nature remains neutral with regard to jurisdictional claims in published maps and institutional affiliations.



Authors and Affiliations

Seung Jae Lee¹ · Moochul Shin² · Chang Hoon Lee² · Priya Tripathi¹

- Seung Jae Lee sjlee@fiu.edu
- Department of Civil and Environmental Engineering, Florida International University, Miami, FL, USA
- Department of Civil and Environmental Engineering, Western New England University, Springfield, MA, USA

